Plant Biotechnology Journal
Open Access

Plant Biotechnology Journal (2023) **21**, pp. 646–661 doi: 10.1111/pbi.13979

Potato protein tyrosine phosphatase StPTP1a is activated by StMKK1 to negatively regulate plant immunity

Fangfang Li[1,†], Xiaokang Chen[1,†], Ruixin Yang[1], Kun Zhang[1], Weixing Shan[2], Matthieu H. A. J. Joosten[3] and Yu Du[1,*]

[1]*State Key Laboratory of Crop Stress Biology for Arid Areas and College of Horticulture, Northwest A&F University, Yangling, Shaanxi, China*
[2]*State Key Laboratory of Crop Stress Biology for Arid Areas and College of Agronomy, Northwest A&F University, Yangling, Shaanxi, China*
[3]*Laboratory of Phytopathology, Wageningen University, Wageningen, The Netherlands*

Received 18 August 2022;
revised 25 November 2022;
accepted 9 December 2022.
**Correspondence* (Tel +86 029-87082613; fax +86 029-87082613; email yu.du@nwafu.edu.cn)
[†]These authors contribute equally to this work.

Keywords: *Phytophthora infestans*, potato, MAPK, resistance, oomycete.

Summary

Phytophthora infestans causes severe losses in potato production. The MAPK kinase StMKK1 was previously found to negatively regulate potato immunity to *P. infestans*. Our results showed that StMKK1 interacts with a protein tyrosine phosphatase, referred to as StPTP1a, and StMKK1 directly phosphorylates StPTP1a at residues Ser-99, Tyr-223 and Thr-290. StPTP1a is a functional phosphatase and the phosphorylation of StPTP1a at these three residues enhances its stability and catalytic activity. StPTP1a negatively regulates potato immunity and represses SA-related gene expression. Furthermore, StPTP1a interacts with, and dephosphorylates, the StMKK1 downstream signalling targets StMPK4 and −7 at their Tyr-203 residue resulting in the repression of salicylic acid (SA)-related immunity. Silencing of *NbPTP1a* + *NbMPK4* or *NbPTP1a* + *NbMPK7* abolished the plant immunity to *P. infestans* caused by *NbPTP1a* silencing, indicating that PTP1a functions upstream of NbMPK4 and NbMPK7. StMKK1 requires StPTP1a to negatively regulate SA-related immunity and StPTP1a is phosphorylated and stabilized during immune activation to promote the de-phosphorylation of StMPK4 and −7. Our results reveal that potato StMKK1 activates and stabilizes the tyrosine phosphatase StPTP1a that in its turn de-phosphorylates StMPK4 and −7, thereby repressing plant SA-related immunity.

Introduction

Plants have evolved plasma membrane-localized receptor-like proteins (RLPs) and receptor-like kinases (RLKs), which are known as pattern recognition receptors (PRRs), to fend off plant pathogens. PRRs monitor the presence of extracellular immunogenic patterns (ExIPs), such as bacterial flagellin to activate pattern-triggered immunity (PTI) (van der Burgh and Joosten, 2019). The detection of an immunogenic pattern (IP) at the cell surface leads to the swift phosphorylation of cytoplasmic mitogen-activated protein kinase (MAPK) cascade proteins through intermediate receptor-like cytoplasmic kinases (RLCKs) and subsequent activation of defence-related gene expression (Bi *et al*., 2018). Upon immune activation, upstream mitogen-activated protein (MAP) kinase kinases (MAPKKKs) are activated by phosphorylation and through phosphorelay, the signal is sequentially transduced to downstream MAP kinase kinases (MAPKKs) and MAP kinases (MAPKs). In Arabidopsis two MAPK cascades, the MKKK-MKK4/5-MPK3/6 and MEKK1-MKK1/2-MPK4 cascades, are known to participate in plant immunity (Zhang *et al*., 2017).

MAPK cascades participate in various processes, including plant development, cell differentiation and the response of the plant to biotic and abiotic stresses (Zhang and Zhang, 2022). For example, the OsMKKK70-OsMAPK6 regulates grain size and leaf angle in rice (Liu *et al*., 2021). The constitutively activated (CA) CA-StMPK7 of potato leads to salicylic acid (SA)-related cell death (Zhang *et al*., 2021). Overexpression of *Arabidopsis thaliana* (Arabidopsis) AtMKK7 and AtMKK9 leads to an *SGT1*-dependent cell death (Popescu *et al*., 2009). Several MAPK cascade proteins have been found to regulate the balance between plant growth and immunity. *Arabidopsis mekk1*, *mkk1 mkk2*, and *mpk4* mutant plants exhibit extreme dwarfism and autoimmune phenotype, and disruption of the MEKK1-MKK1/2-MPK4 cascade activates immunity mediated by the CC-NLR protein SUMM2 (Gao *et al*., 2008; Zhang *et al*., 2012). Therefore, MAPK signalling needs to be accurately regulated to avoid abnormal plant development and immunity.

Plants employ protein phosphatases to modulate the immune response through dephosphorylation of MAPKs. There are three types of protein phosphatases (PPs) in plants, the Ser/Thr-specific phosphoprotein phosphatases (PPPs), the metallo-dependent protein phosphatases (PPMs), which also dephosphorylate Ser/Thr residues, and the protein tyrosine phosphatases (PTPases), which dephosphorylate tyrosine residues (Luan, 2003). The PTPase family shares a conserved motif, (I/V)HCXAGXXR(S/T)G, which can be further divided into two groups, based on their phospho-amino acid specificity, known as the PTPs (phospho-tyrosine-specific phosphatases) and DsPTPs (dual-specificity phospho-Thr/Tyr phosphatases) (Luan, 2003). Well-studied examples of DsPTPs are the MAPK phosphatases (MKPs), the cell cycle regulator CELL DIVISION CYCLE 25 (CDC25) and the PHOSPHATASE AND TENSIN HOMOLOGUE (PTEN) (Maehama *et al*., 2001).

Plant PTPases participate in multiple cellular pathways, including plant immunity, abiotic stress signalling and plant

development. Arabidopsis *PTP1* is induced by high-salt conditions and repressed by cold treatment Xu *et al*. (1998). The enhanced defence phenotype of *mkp1ptp1* double mutants requires both MPK3 and MPK6, suggesting that MKP1 and PTP1 together dephosphorylate MPK3/6 to repress plant immunity (Bartels *et al*., 2009). MKP1 promotes plant vascular resistance to *Xanthomonas oryzae pv. Oryzae by* inactivation of MPK3 (Lin *et al*., 2022). Further investigation revealed that AtPTP1 dephosphorylates and inactivates Arabidopsis AtMPK4 and AtMPK6 (Gupta and Luan, 2003; Huang *et al*., 2000; Park *et al*., 2011). Furthermore, poplar (*Populus nigra*) PdPTP1 was found to interact with PdMPK3 and PdMPK6 and to negatively modulate salt tolerance (Lu *et al*., 2020), whereas rice (*Oryza sativa*) OsPTP1/2 were found to dephosphorylate OsMPK6, thereby inhibiting WRKY45 transcription factor activation and repressing rice immunity to the fungal pathogen *Magnaporthe oryzae* (Ueno *et al*., 2015). However, whether potato StPTP1 regulates the activity of MPK proteins and which MPKs are regulated by StPTP1, remains unknown.

Phospho-tyrosine-specific PTPs share functional similarities in plants and animals, but the copy numbers of the encoding genes in plants and animals are surprisingly different, with 38 genes found in the human genome, but only one gene present in Arabidopsis and two genes in Solanaceous plants (Fu *et al*., 2011; Moorhead *et al*., 2009). PTPs have been reported to be inactivated by H_2O_2 in both plants and animals. For example, reactive oxygen species (ROS) were found to inactivate the catalytic activity of Arabidopsis AtPTP1 (Gupta and Luan, 2003), and in animals H_2O_2 inhibits PTP activity, thereby activating the associated MAPK cascades (Lee and Esselman, 2002). Human PTP1B was reported to be multi-phosphorylated by different protein kinases (Dadke *et al*., 2001; Flint *et al*., 1993), and the human T CELL (TC) PTP was found to be phosphorylated at Ser-304 by a cyclin-dependent kinase (CDK) in mitosis, while this phosphorylation did not significantly alter TCPTP phosphatase activity (Bukczynska *et al*., 2004). Although there are no typical tyrosine kinases identified in plants, some plant RLKs are capable of tyrosine phosphorylation (Bojar *et al*., 2014). Phospho-proteomics data show that the relative abundance of phosphorylated tyrosine residues in plants is similar to that in animals (Ahsan *et al*., 2020; Mühlenbeck *et al*., 2021), hereby indicating the important role that tyrosine phosphorylation plays in signalling events in plants. Thus, the role of plant PTPs is probably largely underestimated, and furthermore, how plant PTPs are actually activated remains unknown.

Previously we revealed that the StMKK1 negatively regulates potato immunity to the late blight disease pathogen *Phytophthora infestans* by repressing SA-related immunity (Chen *et al*., 2021; Du *et al*., 2021). However, StMKK1 also activates its downstream signalling partner, the StMPK7 and StMPK4, which in turn activates potato resistance to *P. infestans* (Zhang *et al*., 2021). To investigate the mechanism by which StMKK1 modulates plant immunity through both negative and positive regulation, we used StMKK1 as a bait and screened the protein against a tomato cDNA yeast two-hybrid library. The potato phosphatase StPTP1a was identified as an interacting protein of StMKK1 and here we confirm the interaction between StPTP1a and StMKK1 and provide evidence that StPTP1a is activated by StMKK1 to subvert StMKK1-StMPK7/4 cascade signalling, thereby repressing SA-related immunity.

Results

StPTP1a interacts with StMKK1

To investigate how StMKK1 represses plant immunity, we used StMKK1 as a bait to screen against a tomato cDNA yeast-two hybrid (Y2H) library (Du *et al*., 2021). A protein tyrosine phosphatase PTP1 was identified as a candidate interacting protein. We BLASTED the PTP1 protein sequence in the SOL genomics network database (https://solgenomics.net/) and performed a phylogenetic analysis of protein sequences of *Solanaceous* PTP1s. Phylogenetic analysis revealed that, different from Arabidopsis, which has only one PTP1 gene, potato and tomato contain two PTP1 genes that share 72% similarity with each other, and are referred to as PTP1a and PTP1b (Figure S1). We cloned the full-length potato *StPTP1a* and performed a one-to-one Y2H analysis to confirm the interaction of StPTP1a with StMKK1. Indeed, our results confirmed the interaction between StPTP1a and StMKK1 (Figure 1a). An *in planta* interaction was tested by co-immunoprecipitation assays and our results show that StPTP1a indeed interacts with StMKK1 *in planta* (Figure 1b). Firefly luciferase complementation imaging (LCI) assays show that the combination of StPTP1a-nluc with cluc-StMKK1 restored the catalytic activity of luciferase, similar to the positive control StMKK1-nluc and cluc-PITG20303 (Du *et al*., 2021) (Figure 1c).

StPTP1a negatively regulates immunity to *Phytophthora* pathogens

To determine the role of StPTP1a in immunity to *P. infestans*, we transiently expressed StPTP1a-myc and the control GUS-myc, in *N. benthamiana* leaves and performed detached leaf inoculation assays. We observed that *StPTP1a*-expressing leaves developed significantly larger lesions than *GUS-myc*-expressing leaves (Figure 2a–c), indicating that StPTP1a negatively regulates resistance to *P. infestans*. We also inoculated *P. parasitica* and *P. capsici* onto *StPTP1a-myc* leaves and results show that *StPTP1a-myc* expressing leaves developed larger lesions than the control (Figure S2a–f), indicating that StPTP1a negatively regulates immunity to *Phytophthora* pathogens in general. SA-related gene expression was measured by qRT-PCR analysis of *StPTP1a*- or *GUS*-expressing leaves, and the results show that *StPTP1a* expression significantly inhibits *PR1* and *PR2* expression (Figure 2g). The StPTP1a-myc and GUS-myc fusion proteins were properly accumulating *in planta*, as determined by western blotting (Figure S2g). To confirm the role of PTP1a as a negative regulator of plant immunity, we set out to silence *NbPTP1a* in *N. benthamiana* by virus-induced gene silencing (VIGS). From the phylogenetic tree, we observed that *N. benthamiana* appeared to contain three *PTP1* genes (Figure S1). We therefore designed two VIGS constructs to silence the expression of the orthologous genes, with the TRV-*NbPTP1a* construct aimed at silencing the two copies of *NbPTP1a* (*Niben101Scf03425g03015* and *Niben101Scf01365g00010*), while the TRV-*PTP1b* construct was designed to silence the other copy, referred to as *NbPTP1b* (*Niben101Scf04216g01006*). The qRT-PCR analysis showed that *NbPTP1a* and *NbPTP1b* are efficiently silenced in plants (Figure S3b,d) and silencing of *NbPTP1a* or *NbPTP1b* in *N. benthamiana* does not alter plant morphology (Figure S3a,c). When inoculated with *P. infestans*, the *NbPTP1a*- and *NbPTP1b*-silenced plants developed smaller lesions compared to the control (Figure 2d–f and Figure S3f,g), which confirms that PTP1 plays

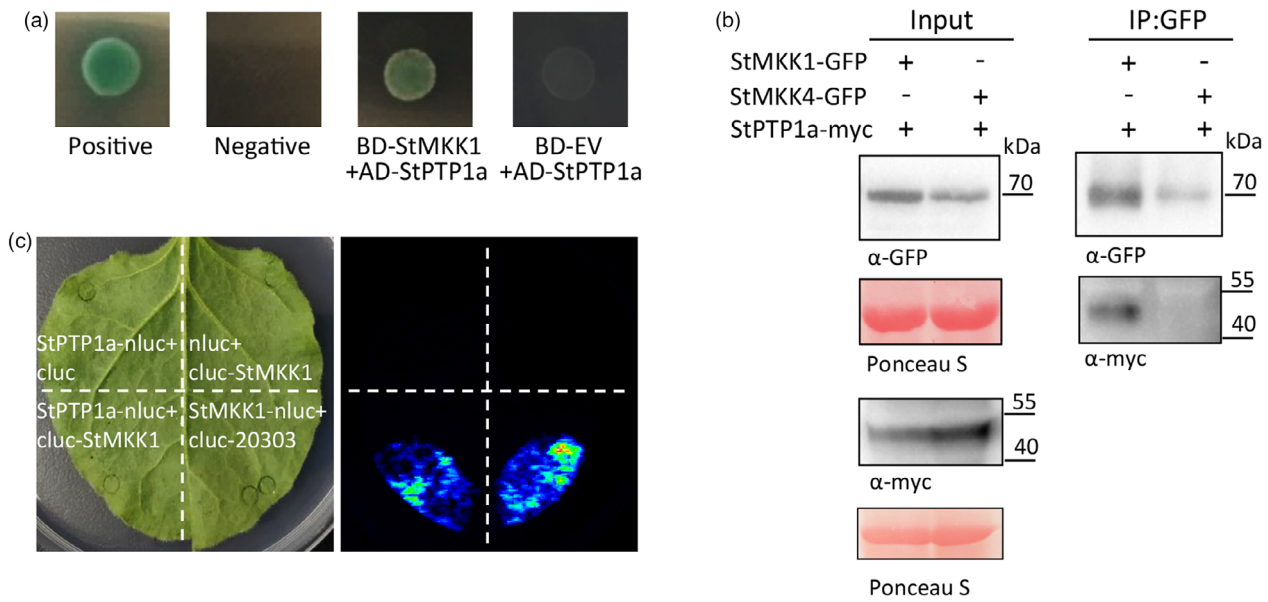

Figure 1 StPTP1a interacts with StMKK1. (a) StMKK1 interacts with StPTP1a in Y2H assays. Yeast co-expressing DNA binding domain (BD)-StMKK1 with activation domain (AD)-StPTP1a and the positive controls as indicated, were grown on TDO medium and α-galactosidase activity was activated, while the negative control and yeast cells co-expressing the BD empty vector with AD-StPTP1a, did not. The positive and negative control were provided by the manufacturer (Matchmaker GAL4 Two-Hybrid System 3, Clontech). (b) Co-immunoprecipitation was performed using GFP-Trap_A beads and confirmed that StPTP1a-myc associates with StMKK1-GFP, while the control, StMKK4-GFP only, (Sotub03g034170.1 was found to belong to the clade C of StMAPKKs and we named it StMKK4) did not. +, indicates that these particular proteins were transiently co-expressed in leaves of *N. benthamiana*. The equal loading of total proteins is indicated by Ponceau staining (Ponceau S). (c) Luciferase complementation imaging (LCI) assays show that StPTP1a interacts with StMKK1. The left picture shows the scheme of the expression of the various fusion proteins, while the right picture shows the occurrence of protein–protein interactions as revealed by the fluorescence signals. Co-expression of StMKK1-nluc and cluc-PITG20303 was used as a positive control. The experiments were repeated three times with similar results.

a negative role in the immunity of *Solanaceous* plants to *P. infestans*. Determination of the level of SA-related gene expression in the TRV-*NbPTP1a*- and TRV-*NbPTP1b*-inoculated plants revealed that these plants exhibited a significantly higher *PR1* and *PR2* expression than the control, indicating that PTP1 negatively regulates SA-related immunity (Figure 2h and Figure S3e). To further explore whether silencing of *StPTP1* in potato also promotes resistance to *P. infestans*, we generated *StPTP1*-RNAi construct, which targets both *PTP1a* and *-b* paralogous genes and transformed potato cultivar Desiree using agrobacterium-mediated transformation. Two independent transgenic lines were generated, and we observed that both *StPTP1*-RNAi lines showed a significant reduction in *StPTP1* transcript levels (>80%) (Figure 2j). However, both *StPTP1*-silenced potato transgenic lines showed strong developmental defects (Figure 2i), which rendered infection assays not possible. Instead, we checked MPK activation after treatment with the bacterial PAMP flg22 and observed that the *StPTP1*-silenced potato lines exhibited enhanced MPK6/3 activation when compared to the control (Figure 2k). We tested SA-related gene expression in the *StPTP1*-RNAi lines. The results showed that silencing of *StPTP1* in potato enhances SA-related gene expression when compared to the control (Figure 2l).

StMKK1 activates StPTP1a phosphatase activity

To reveal whether StPTP1a encodes a functional protein tyrosine phosphatase, we introduced point mutations for the essential amino acids D243 and C274, which are conserved among the PTPs from potato and Arabidopsis (Figure S4), thereby generating the MBP-StPTP1aAS (StPTP1a$^{D243A,\ C274S}$) construct. The MBP-StPTP1a, MBP-GFP and MBP-StPTP1aAS proteins were expressed and purified from *Escherichia coli*, and were separated on SDS-PAGE gels (Figure S5a). The purified proteins were subjected to protein phosphatase assays with p-nitrophenyl phosphate (pNPP) as a substrate. A yellow nitrophenol product was generated in the presence of StPTP1a, but not in the presence of the negative control GFP or StPTP1aAS (Figure S5b). The yellow nitrophenol product was quantified using a microplate reader at the absorbance of 405 nm (A405) and we observed that StPTP1a hydrolysed pNPP rapidly, as shown by an increased absorbance, which is in contrast to the negative controls, of which the absorbance of the solution remained at a basic level (Figure 3a). This result indicates that StPTP1a is indeed an active phosphatase and that mutation of the amino acids that are essential for its activity indeed abolishes its enzymatic activity. To investigate whether StMKK1 affects the phosphatase activity of StPTP1a as a result of its phosphorylation, an *in vitro* phosphorylation was performed by incubation of StPTP1a with His-StMKK1, the kinase dead His-StMKK1 (StMKK1^{K99M}; Du *et al*., 2021) and His-GFP, after which the MBP-StPTP1a fusion protein was tested for phosphatase activity. StPTP1a that incubated with His-StMKK1 hydrolysed pNPP more rapidly than the negative controls (Figure 3b), and to confirm that actual phosphorylation of StPTP1a by StMKK1 had taken place, the His-GFP or His-StMKK1 proteins were incubated with His-MBP-StPTP1a and *in vitro* phosphorylation assays were performed. For this, the phosphorylated StPTP1a proteins were separated on SDS-PAGE gels, supplemented with phos-tag (100 μM, FUJIFILM Wako Cat: AAL-107), and it was observed that phosphorylation of StPTP1a is

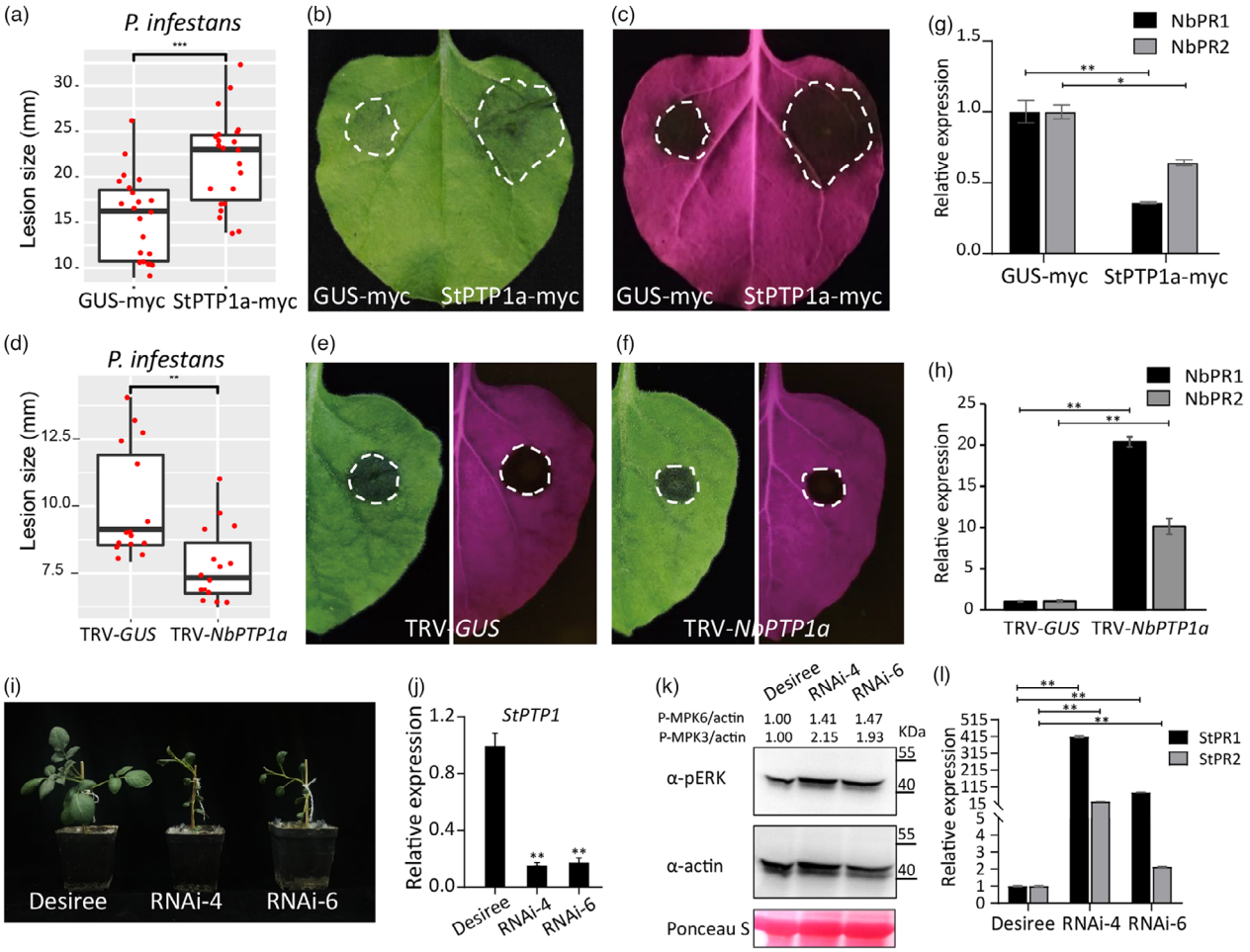

Figure 2 StPTP1a Negatively regulates immunity to *P. infestans*. (a, d) Bar graphs show that overexpression of StPTP1a and silencing of *NbPTP1a*, respectively suppresses and enhances resistance to *P. infestans*. The lesion diameters were determined at 6 days after pathogen inoculation (dai), and the average lesion diameters (mm) are shown in the boxplots. Error bars from (a, d) indicate the standard errors (one-sided Student's *t*-test, two stars indicate $P \leq 0.01$; three star indicates $P \leq 0.001$; $n \geq 15$). (b, c, e, f) Representative images showing the lesions that developed on the GUS-myc and the StPTP1a-myc agroinfiltrated (b, c) and *GUS*- and *NbPTP1a*-silenced (e, f) *N. benthamiana* leaves. Left pictures were taken under normal light, while the right pictures were taken under blue light. (g, h) PTP1a suppresses SA-related immune signalling. Bar graphs showing *PR* gene expression in *StPTP1a-myc* overexpressing (g) and *NbPTP1a*-silenced (h) leaves. The expression level of the *N. benthamiana actin* gene was used for normalization. (i) Morphology of *StPTP1-RNAi*-transgenic potato lines at 5 weeks after planting. (j) The silencing efficiency of *StPTP1* in *StPTP1-RNAi*-transgenic potato lines. The expression level of *StPTP1* in untreated Desiree was used as a control. (k) Leaves of *StPTP1-RNAi*-transgenic lines were treated with 20 μM flg22, after which they were harvested and total proteins were extracted at 15 min after treatment. The phosphorylation levels of the MPK3/6 proteins were determined using anti-pERK antibodies. Equal loading of total proteins is indicated by Ponceau staining. Numbers above the blot indicate the relative intensity of phosphorylated MPK6 or MPK3 to plant actin normalized to Desiree control. (l) Relative expression of *PR1* and *PR2* genes in stable *StPTP1-RNAi*-transgenic potato lines. The expression of the potato *actin* gene was used for normalization. Error bars from (g, h, j, l) indicate the standard error from 3 technical replicates. Asterisks indicate significant differences (one-sided Student's *t*-test, *, $P \leq 0.05$, **, $P \leq 0.01$). The experiments showed similar patterns in three biological replicates.

enhanced upon incubation with His-StMKK1 showing by an increased insensitive of the upper bands of StPTP1 (Figure 3c). To further investigate which amino acid residues of StPTP1a are phosphorylated by StMKK1, we performed a mass spectrometry (MS) analysis of MBP-StPTP1a, after its *in vitro* phosphorylation by StMKK1. We observed that the Ser-99, Tyr-223 and Thr-290 residues in MBP-StPTP1a are directly phosphorylated by StMKK1 (Figure 3d). Thereafter, we replaced these three residues by the amino acid Ala and generated the MBP-StPTP1a^{S99A}, MBP-StPTP1a^{Y223A}, MBP-StPTP1a^{T290A} and MBP-StPTP1a^{S99AY223AT290A} mutant proteins. Phosphatase assays revealed that MBP-StPTP1a^{S99A}, MBP-StPTP1a^{Y223A} and MBP-StPTP1a^{T290A} retain their phosphatase activity and are activated by StMKK1 but not by StMKK1^{K99M}, whereas MBP-StPTP1a^{S99AY223AT290A} does not show any phosphatase activity and can no longer be activated by StMKK1 (Figure 3e–h). Taken together, these results indicate that StMKK1 directly phosphorylates StPTP1a at residues Ser-99, Tyr-223 and Thr-290, and that this phosphorylation activates the enzyme. To investigate whether its phosphatase activity and the phosphorylation of StPTP1 is required for suppression of plant immunity to *P. infestans*, we transiently expressed StPTP1aAS-myc, StPTP1a^{S99A}-myc, StPTP1a^{Y223A}-myc, StPTP1a^{T290A}-myc, StPTP1a^{S99AY223AT290A}-myc and the control GUS-myc in *N. benthamiana* leaves and performed pathogen infection assays. We observed that StPTP1aAS, StPTP1a^{S99A}, StPTP1a^{Y223A}, StPTP1a^{T290A} and StPTP1a^{S99AY223AT290A}-expressing leaves have

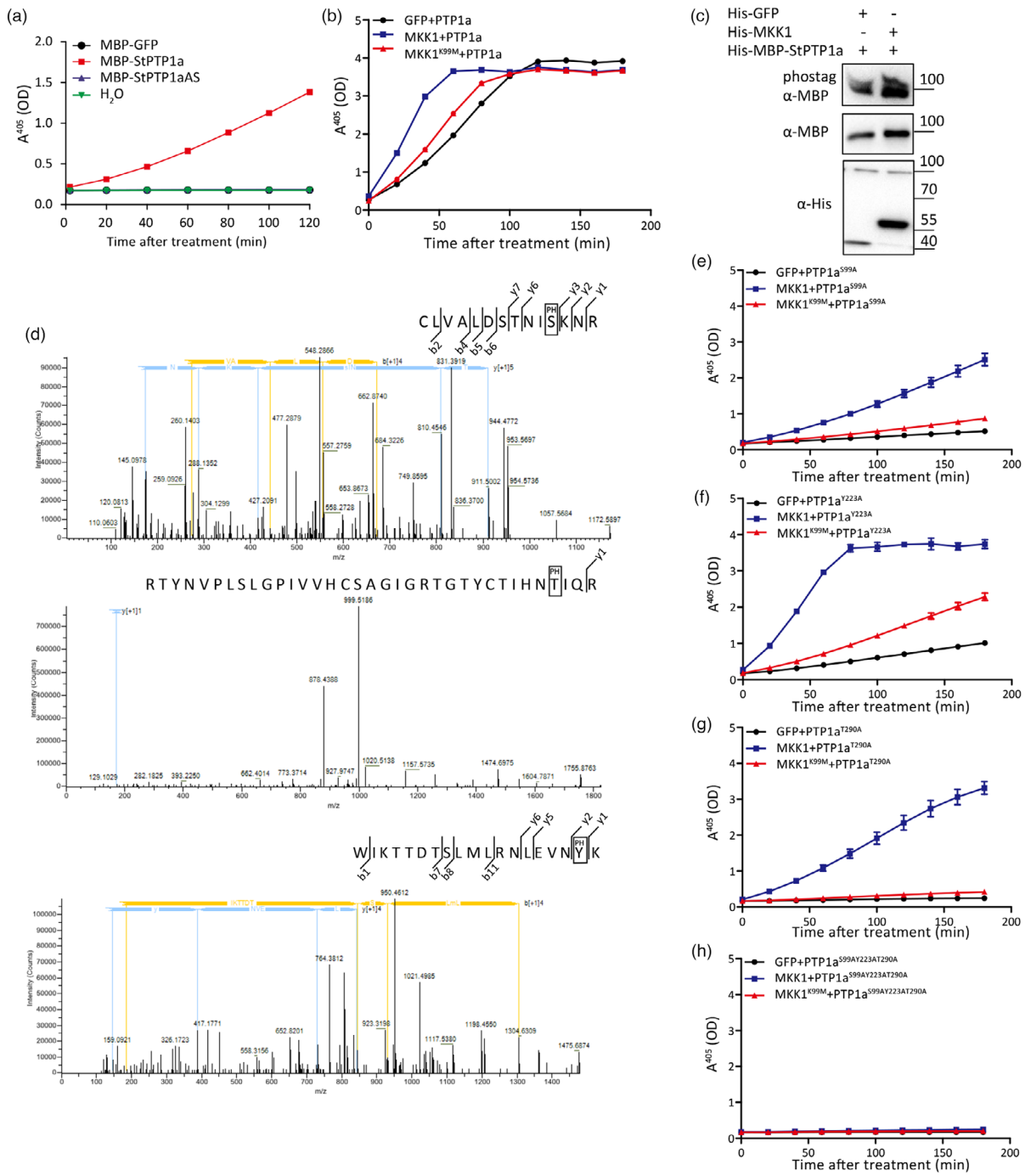

Figure 3 StPTP1a functions as a phosphatase and StMKK1 increases the enzymatic activity of StPTP1a by phosphorylation of the protein at Ser-99, Tyr-223 and Thr-290. (a) StPTP1a is a functional phosphatase. A time course experiment revealing the phosphatase activity of StPTP1a is shown. pNPP was used as a substrate and the yellow nitrophenol product generated by the active phosphatase was quantified over time using a microplate reader at the absorbance of 405 nm (A405). Two μg of *E. coli*-produced, purified His-MBP-GFP, His-MBP-StPTP1a and His-MBP-StPTP1aAS proteins were used in the assay. (b) Incubation of StPTP1a with StMKK1 but not StMKK1^{K99M} increases the phosphatase activity of StPTP1a. A time course experiment revealing the increased phosphatase activity of His-MBP-StPTP1a upon incubation with His-StMKK1 but not with the kinase dead mutant His-StMKK1^{K99M} is shown. pNPP was used as a substrate and the yellow nitrophenol product generated by the active phosphatase was quantified over time using a microplate reader at the absorbance of 405 nm (A405). One μg of His-StMKK1, His-StMKK1^{K99M}, His-GFP and His-MBP-StPTP1a was used in the assay. (c) StPTP1a phosphorylation is enhanced when incubated with StMKK1. His-MBP-StPTP1a was incubated with either His-GFP or His-MKK1, and *in vitro* kinase assays were performed. Phosphorylated StPTP1a was subsequently separated on gel supplemented with phos-tag, and was detected using α-MBP antibody. The α-His blot shows all the His-tagged proteins. (d) StPTP1a is phosphorylated by StMKK1 in *in vitro* at Ser-99, Tyr-223 and Thr-290. The LC–MS/MS spectra of the phospho-peptides of StPTP1a containing phosphorylated Ser-99, Tyr-223 and Thr-290 sites are shown. (e–h) The graphs show the time course of the phosphatase activity of StPTP1a^{S99A}, StPTP1a^{Y223A}, StPTP1a^{T290A} and StPTP1a^{S99AY223AT290A}, incubated with His-StMKK1, His-StMKK1^{K99M} or His-GFP. One ug of each of the proteins was used in the assay. The experiments were repeated three times with similar results.

lost their ability to promote *P. infestans* colonization when compared to GUS-myc-expressing leaves (Figure S6). These results indicate that both the phosphatase activity of StPTP1a and the phosphorylation of StPTP1a by StMKK1 are essential for its role in immune suppression.

StPTP1a interacts with, and dephosphorylates, StMPK4 and StMPK7

To identify possible *in planta* targets of StPTP1a, we transiently expressed StPTP1a-GFP in *N. benthamiana* leaves, and immunoprecipitated StPTP1a-GFP at 2 dpi and subsequently performed MS analysis. We identified NbMKK1, NbMPK4, NbWIPK and NbSIPK as StPTP1a co-purifying proteins. We cloned potato *StSIPK*, *StMPK4* and the close homologue of *StMPK4*, *StMPK7* (Zhang *et al*., 2021), and checked whether StPTP1a interacts with StMPK4 and StMPK7 in a co-immunoprecipitation experiment. We observed that StMPK7 and StMPK4 specifically interact with StPTP1a (Figure 4a,b). The interaction was further confirmed by LCI, and results show that the combination of StPTP1a-nluc with cluc-StMPK7 or cluc-StMPK4 restored the catalytic activity of luciferase (Figure 4c,d), similar to the positive control consisting of the combination StMKK1-nluc with cluc-20 303 (Du *et al*., 2021).

To test whether StMPK7 activates StPTP1a, an *in vitro* phosphorylation assay was performed by incubating GST-GFP or GST-StMPK7 with the MBP-StPTP1a protein. We observed that incubation of GST-StMPK7 with StPTP1a does not enhance StPTP1a phosphatase activity, when compared to the control (Figure 4e). To investigate whether StPTP1a dephosphorylates StMPK7, we transiently expressed GFP-StMPK7 in combination with GUS-myc, StPTP1a-myc or StPTP1aAS-myc, in *N. benthamiana* leaves and treated the agroinfiltrated leaves with flg22 at 2 dpi. Samples were harvested at 0 and 15 min after flg22 treatment and total proteins were extracted. Results showed that at 0 min after flg22 treatment the MPK proteins were not activated, while at 15 min after flg22 treatment MPK7/6/3 were activated by phosphorylation. We observed a significant reduction in StMPK7 phosphorylation when co-expressed with StPTP1a, when compared to co-expression with GUS-myc or the mutated StPTP1aAS control (Figure 4f). However, a significant induction in StMPK7 phosphorylation was observed at 15 min after flg22 treatment in TRV-*PTP1a* plants compared with the control TRV-*GUS* plants (Figure S10a). These results indicate that StPTP1a indeed dephosphorylates StMPK7. To further confirm this, *in vitro* phosphorylation assays were performed. We observed that StMPK7 is phosphorylated by StMKK1 *in vitro*; however, StPTP1a significantly dephosphorylates StMPK7, while the catalytically inactivated StPTP1aAS mutant only weakly dephosphorylated StMPK7 (Figure 4g). The α-pERK specifically detects the Thr-202 and Tyr-204 residues in MPKs, and as the tyrosine-specific protein phosphatase, we therefore suspect that StPTP1a may dephosphorylate StMPK7 specifically at the conserved Tyr-203 residue. We confirmed dephosphorylation at the Tyr-203 residue by generating the StMPK7^{Y203A} mutant, and the dephosphorylation of StMPK7 and StMPK7^{Y203A} by StPTP1a was detected *in planta*. We found that StMPK7^{Y203A} completely lost the ability to be phosphorylated when PTI was triggered, indicating that Tyr-203 is the essential residue for the activation of StMPK7 by phosphorylation (Figure 4h). To determine possible dephosphorylation of StMPK7 by StPTP1a-myc, StPTP1a^{S99A}-myc, StPTP1a^{Y223A}-myc, StPTP1a^{T290A}-myc and StPTP1a^{S99AY223AT290A}-myc, we co-expressed GFP-StMPK7 with GUS-myc, StPTP1a, or with one of the mutated forms of StPTP1a. At 2 dpi the leaves were infiltrated with 10 μM flg22, and subsequently total proteins were extracted at 15 min after flg22 treatment. We observed that mutation of any of these three phosphorylation sites does not reduce the ability of StPTP1a to dephosphorylate StMPK7 (Figure 4i), while StPTP1a^{S99AY223AT290A}-myc have lost its ability to dephosphorylate StMPK7 (Figure 4j). These results indicate that the three residues, Ser-99, Tyr-223 and Thr-290 are likely functional redundant for the enzymatic activity of StPTP1a.

Since activation of StMPK7 leads to programmed cell death, we co-expressed constitutively activated CA-StMPK7 (Zhang *et al*., 2021) with StPTP1a or the negative control GUS, while co-expression of INF1 with GUS or StPTP1a was used as an additional control. We observed that StPTP1a represses the CA-StMPK7-triggered cell death, whereas GUS did not (Figure S7a). INF1-triggered cell death was not affected upon co-expression of StPTP1a. DAB staining was performed to visualize the H_2O_2 accumulation in the agroinfiltrated sites and it was clear that at the CA-StMPK7- and INF1-agroinfiltrated sites generated large amounts of H_2O_2, whereas when StPTP1a was co-expressed, CA-StMPK7 triggered significantly less H_2O_2 accumulation (Figure S7b). Cell death was quantified by ion leakage measurements, and the results confirmed our observation that StPTP1a

Figure 4 StPTP1a interacts with, and dephosphorylates, StMPK7. (a, b) StPTP1a associates with StMPK7 (a) and StMPK4 (b). Co-immunoprecipitation was performed using GFP-Trap_A beads and confirmed that GFP-tagged StPTP1a associates with myc-StMPK7 and StMPK4-myc, while the control GFP only does not. +, indicates that the proteins were transiently expressed in leaves of *N. benthamiana*. (c, d) LCI confirms that StPTP1a interacts with StMPK7 (c) and StMPK4 (d). The left picture shows the scheme of the expression of the various fusion proteins, while the right picture shows the occurrence of protein–protein interactions by the fluorescence signals. Co-expression of StMKK1-nluc and cluc-20 303 was used as a positive control. (e) StPTP1a phosphatase activity is not affected upon incubation with StMPK7. A time course experiment determining the phosphatase activity of His-MBP-StPTP1a, incubated with either GST-GFP or GST-StMPK7 is shown. One μg of the GST-StMPK7, GST-GFP and MBP-StPTP1a proteins was used in the assay. (f) StPTP1a, but not StPTP1aAS, dephosphorylates StMPK7 *in vivo*. GFP-StMPK7 (f) or mutated GFP-StMPK7^{Y203A} (h) was co-agroinfiltrated with GUS-myc, StPTP1a-myc or StPTP1aAS-myc in *N. benthamiana* leaves. At 2 dpi the leaves were treated with flg22, and total proteins were extracted at 0 and 15 min after flg22 treatment. Phosphorylation of MPK3/6/7 proteins was detected using anti-pERK antibodies. (h) There was no phosphorylation signal detected for GFP-StMPK7^{Y203A}. (g) *In vitro* kinase assays show that StPTP1a, but not StPTP1aAS, dephosphorylates StMPK7. The recombinant proteins His-StMKK1 and GST-StMPK7 were incubated with His-MBP-GFP, His-MBP-StPTP1a, or His-MBP-StPTP1aAS and phosphorylation of the MPK7 protein was detected using α-pERK antibodies. (i) Dephosphorylation of StMPK7 by StPTP1a^{S99A}, StPTP1a^{Y223A} and StPTP1a^{T290A} upon flg22 treatment. Flg22 was infiltrated at 2 dpi and total proteins were extracted at 15 min after flg22 treatment. Protein loading is indicated using Ponceau Staining. (j) Dephosphorylation of StMPK7 by StPTP1a^{S99AY223AT290A} upon flg22 treatment. Flg22 was infiltrated at 2 dpi and total proteins were extracted at 15 min after flg22 treatment. Numbers indicate the relative intensity of phosphorylated StMPK7 versus GFP-StMPK7 or GST-StMPK7 normalized to GUS or MBP control (f, g, i, j). The recombinant fusion proteins of StPTP1a and mutations of StPTP1a are marked with black asterisks in (f, h, i, j). The experiments were repeated three times with similar results.

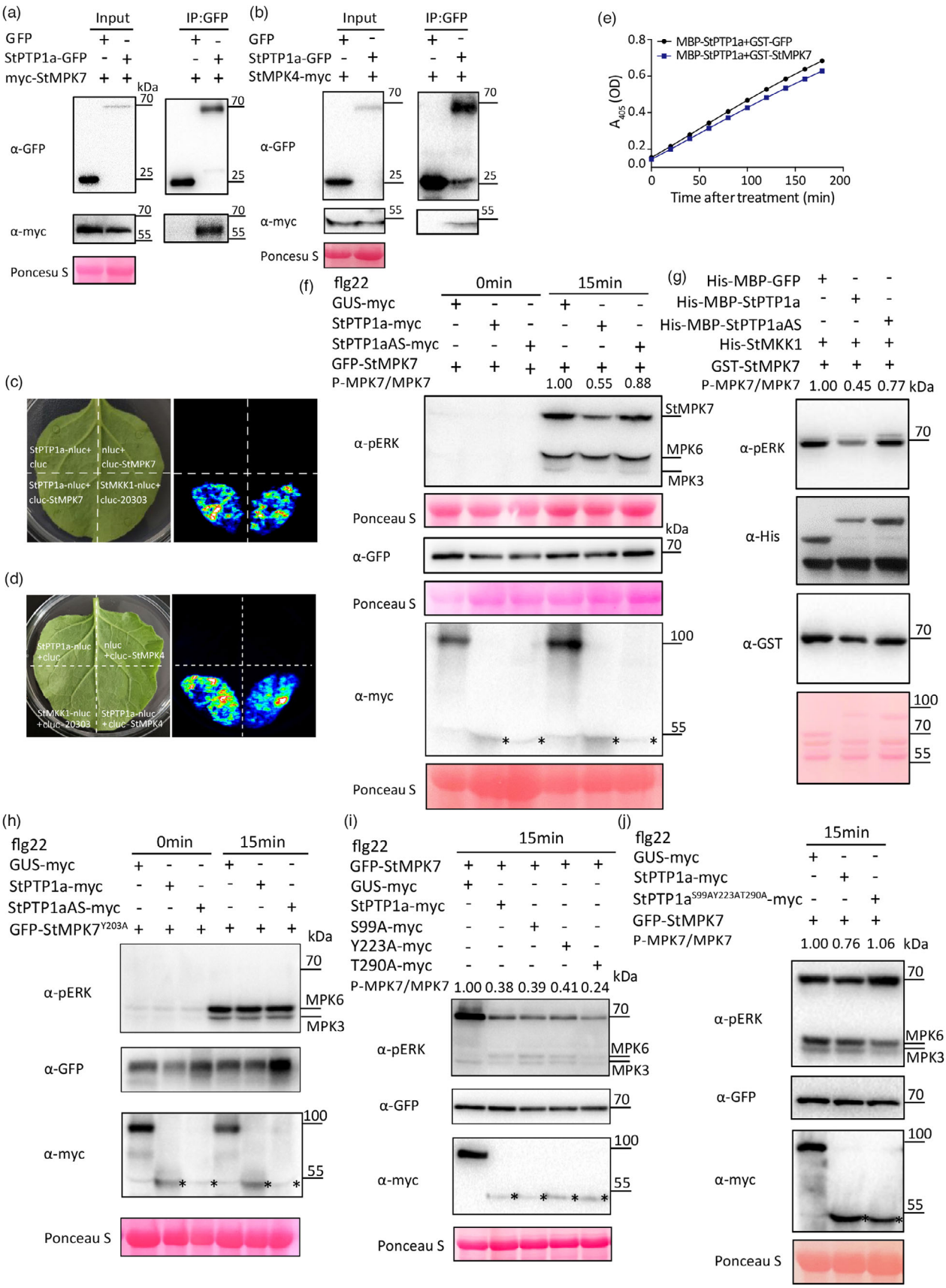

significantly represses CA-StMPK7-triggered cell death (Figure S7c).

To further investigate whether StPTP1a inhibits StMPK7-mediated immunity to *P. infestans*, GUS-GFP or StPTP1a-GFP were co-expressed with either GUS-GFP or GFP-StMPK7, and at 2 dpi the leaves were harvested for *P. infestans* inoculation. When co-expressed with GUS-GFP, GFP-StMPK7 significantly promotes resistance to *P. infestans* as shown by smaller lesion areas (Figure S7d,e). However, when co-expressed with StPTP1a-GFP, GFP-StMPK7 loses its ability to enhance immunity to *P. infestans* (Figure S7d,f). Silencing of both *NbMPK7* and *NbPTP1a* in *N. benthamiana* hampered the *NbPTP1a*-silencing-induced resistance to *P. infestans*, confirming our observation that NbMPK7 activity is regulated by NbPTP1 (Figure S7g,h). The qRT-PCR analysis showed that *NbMPK7* and *NbPTP1a* are efficiently silenced in plants (Figure S7i,j). To check whether Tyr-203 of StMPK7 is essential for CA-StMPK7-mediated cell death, we generated the CA-StMPK7^{Y203A}-myc and agroinfiltrated it into *N. benthamiana* leaves. The results show that CA-StMPK7^{Y203A}-myc no longer triggers cell death, although it still triggers H_2O_2 accumulation (Figure S7k–m). GFP-StMPK7^{Y203A} is also not functional anymore in promoting resistance to *P. infestans*, as no difference in lesion size was observed when GFP-StMPK7^{Y203A} was agroinfiltrated next to GUS control (Figure S7n,o).

AtPTP1 was reported previously to dephosphorylate AtMPK6 and AtMPK4, and this dephosphorylation almost completely abolished AtMPK4 catalytic activity (Huang *et al.*, 2000; Park *et al.*, 2011). To confirm whether the situation is the same for potato, the potato functional orthologues of MPK4 (StMPK4-GFP, PGSC0003DMP400000144), MPK6 (StSIPK-GFP, KJ027596) and MPK3 (StWIPK-GFP, PGSC0003DMP400052344), were co-expressed with either GUS-myc or StPTP1a-myc in *N. benthamiana* leaves. At 2 dpi, the leaves were harvested upon a 15 min treatment with flg22, and total proteins were extracted. We observed that StMPK4 was activated when co-expressed with GUS-myc, but not when co-expressed with StPTP1a-myc (Figure 5a), similar to the result of MPK7, StMPK4 was activated at 15 min after flg22-treatment in TRV-*PTP1a* plants compared with the control TRV-*GUS* plants (Figure S10b), which indicates that StPTP1a dephosphorylated StMPK4. However, StPTP1a did neither dephosphorylate StSIPK, nor StWIPK (Figure 5b,c). *In vitro* phosphorylation assays also confirmed that StPTP1a significantly dephosphorylates StMPK4, while the catalytically inactivated StPTP1aAS mutant only weakly dephosphorylated StMPK4 (Figure 5d). Further *in planta* investigations showed that the mutated StPTP1a proteins, StPTP1a^{S99A}, StPTP1a^{Y223A} and StPTP1a^{T290A}, partially retained the ability to dephosphorylate StMPK4, while StPTP1a^{S99AY223AT290A} has completely lost its ability to dephosphorylate StMPK4 (Figure 5e,g). In addition, StMPK4^{Y203A} completely lost the ability to be phosphorylated when PTI was triggered, indicating that Tyr-203 is the essential residue for the activation of StMPK4 by phosphorylation (Figure 5f). StPTP1a represses CA-StMPK4-triggered cell death and mutation of the Tyr-203 residue to Ala abolished the CA-StMPK4-triggered cell death and StMPK4-mediated immunity (Figure 5h–k). In addition, we also found that silencing of both *NbMPK4* and *NbPTP1a* in *N. benthamiana* abolished the *NbPTP1a*-silencing-induced resistance to *P. infestans*, which indicates that NbMPK4 functions downstream of NbPTP1a (Figure 5l,m). The qRT-PCR analysis showed that *NbMPK4* and *NbPTP1a* are efficiently silenced in plants (Figure 5n,o). Taken together, StPTP1a shows a strong dephosphorylation specificity for StMPK4 and StMPK7 at their Tyr-203 residue, but has almost no dephosphorylation activity for StSIPK and StWIPK.

Upon activation of PTI, StPTP1a is phosphorylated and stabilized to repress StMPK4 and StMPK7 activation

To investigate the stability of the StPTP1a protein during the PTI response, we transiently expressed StPTP1a-GFP in *N. benthamiana* leaves and at 2 dpi the leaves were treated with flg22. Total

Figure 5 StPTP1a represses the phosphorylation of StMPK4 but does not affect the phosphorylation status of StSIPK or StWIPK. (a-c) StPTP1a dephosphorylates StMPK4 (in a, the co-infiltration of StPTP1a and StMPK4 was done in triplicate), but not StSIPK or StWIPK. StMPK4-GFP, StSIPK-GFP or StWIPK-GFP was co-infiltrated with either GUS-myc or StPTP1a-myc into *N. benthamiana* leaves. At 2 dpi the leaves were treated with flg22, and total proteins were extracted 15 min later. The phosphorylation status of the StMPK4, StSIPK and StWIPK proteins was determined using anti-pERK antibodies. In b, + indicates an OD of all Agrobacterium suspensions of 0.4, ++ indicates an OD of 0.8, and +++ indicates an OD of 1.2. (d) *In vitro* kinase assays show that StPTP1a, but not StPTP1aAS, dephosphorylates StMPK4. The recombinant proteins His-StMKK1 and GST-StMPK4 were incubated with His-MBP-GFP, His-MBP-StPTP1a, or His-MBP-StPTP1aAS, and phosphorylation of the StMPK4 protein was detected using α-pERK antibodies. (e) StPTP1a^{S99A}, StPTP1a^{Y223A} and StPTP1a^{T290A} have a slightly reduced ability to dephosphorylate StMPK4 upon flg22 treatment. Flg22 was infiltrated at 2 dpi and total proteins were extracted at 15 min after flg22 treatment. (f) StMPK4^{Y203A}-GFP is not phosphorylated upon flg22 treatment. The co-expression of the proteins is indicated with +. Flg22 was infiltrated at 2 dpi and total proteins were extracted at 15 min after flg22 treatment. (g) StPTP1a^{S99AY223AT290A} cannot dephosphorylate StMPK4. Flg22 was infiltrated at 2 dpi and total proteins were extracted at 15 min after flg22 treatment. The equal loadings of total proteins are indicated by Ponceau staining (a-g). Numbers indicate the relative intensity of phosphorylated StMPK4 versus StMPK4-GFP or GST-StMPK4 normalized to GUS or MBP control (d, e, g). The recombinant fusion proteins of StPTP1a and mutations of StPTP1a are marked with black asterisks in (a, b, c, e, f, g). (h) CA-StMPK4 or INF1 was co-expressed either with StPTP1a or GUS in leaves of *N. benthamiana*. The picture shown on the left was taken at 5 dpi. The ratios indicate the amount of agroinfiltrated sites showing cell death versus the total amount of agroinfiltrated sites, from two independent experiments, at 5 dpi. Mock indicates the infiltration of Agrobacterium only. The picture shown on the right illustrates the DAB staining of the same leaf, which shows strong H_2O_2 accumulation at the CA-StMPK4- and INF1-agroinfiltrated sites. (i) CA-StMPK4^{Y203A} has lost its ability to trigger cell death. The leaves were photographed at 5 dpi. (j, k) Overexpression of the StMPK4^{Y203A} mutant does not trigger increased immunity to *P. infestans*. Representative images, showing lesion development on the agroinfiltrated leaves are shown (j). Lesion diameters were determined at 6 dai, and the average lesion areas (mm^2) are shown in the graphs (k). (l, m) Silencing of both *NbMPK4* and *NbPTP1a* in *N. benthamiana* represses the *NbPTP1a*-silencing induced plant resistance, indicating that NbMPK4 activity is regulated by NbPTP1. Representative images taken under blue light, showing lesion development on the leaves are shown (l). Lesion diameters were determined at 6 dai, and the average lesion areas (mm^2) are shown in the graphs (m). Error bars indicate the standard error from at least 10 technical replicates. Significance is indicated with asterisks ($n \geq 10$; one-sided Student's *t*-test, two stars indicate $P \leq 0.01$). The experiments were repeated at least two times, with similar results. (n, o) Relative quantification (RQ) of *NbMPK4* and *NbPTP1a* expression in TRV-*GUS*- and TRV-*NbMPK4* + TRV-*NbPTP1a*-inoculated plants. Error bars indicate the standard error from three technical replicates. Asterisks indicate significant differences (one-sided Student's *t*-test, *, $P \leq 0.05$, **, $P \leq 0.01$).

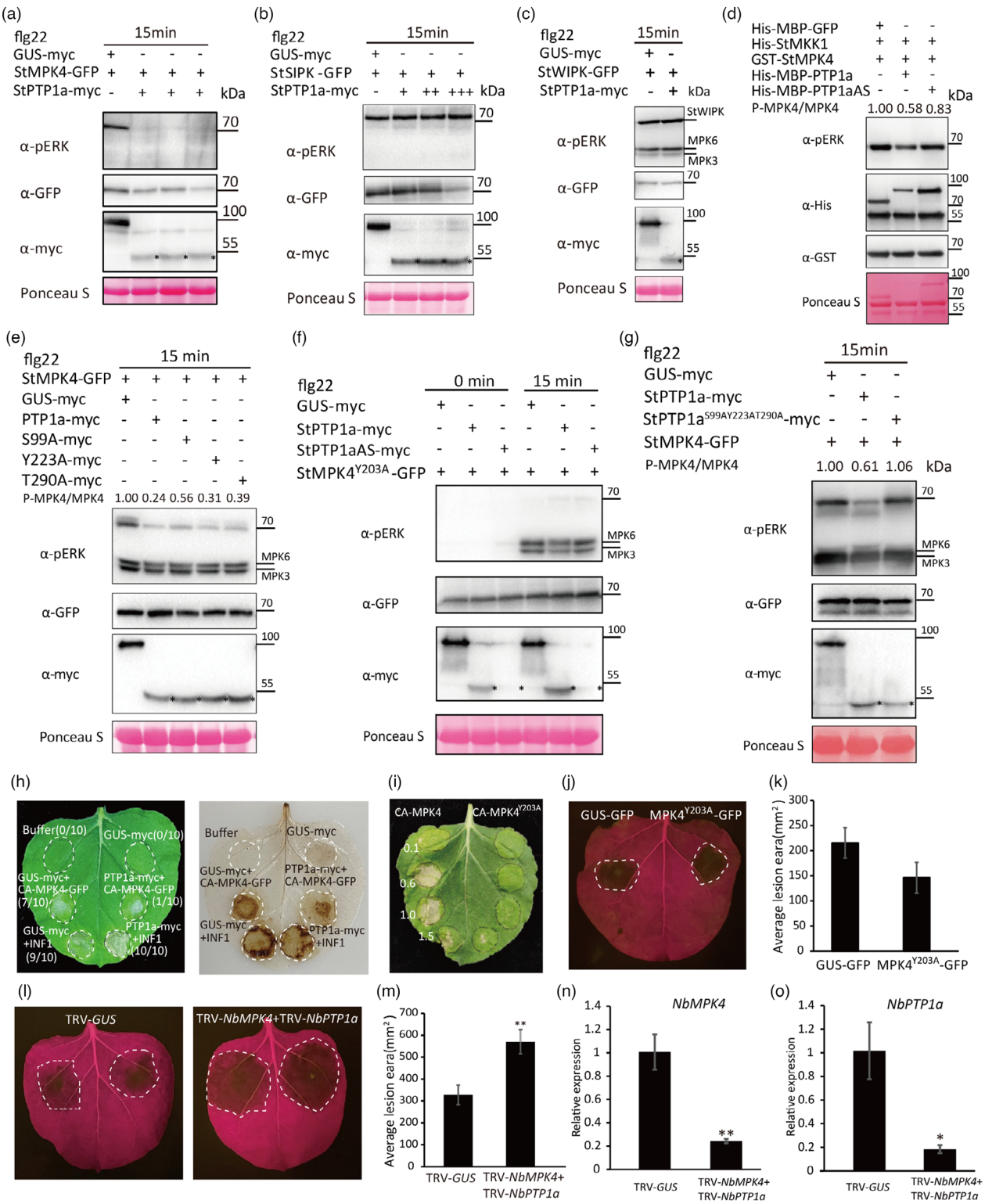

proteins were extracted at different time points after flg22 treatment. Western blots show that the StPTP1a-GFP protein is stable upon mounting of PTI, although induced mobility of the protein was observed, starting from 15 min after PTI elicitation and with the biggest mobility shift at 45 min after PTI elicitation (Figure 6a). This electrophoretic mobility shift of StPTP1a-GFP is likely due to increased phosphorylation and to proof this, we treated the protein extracts with calf intestine alkaline phosphatase (CIAP), and the treated samples were again separated on SDS-PAGE gels. The band shift was not observed anymore in CIAP-treated samples, confirming that phosphorylation is indeed responsible for the lower mobility of the StPTP1a protein

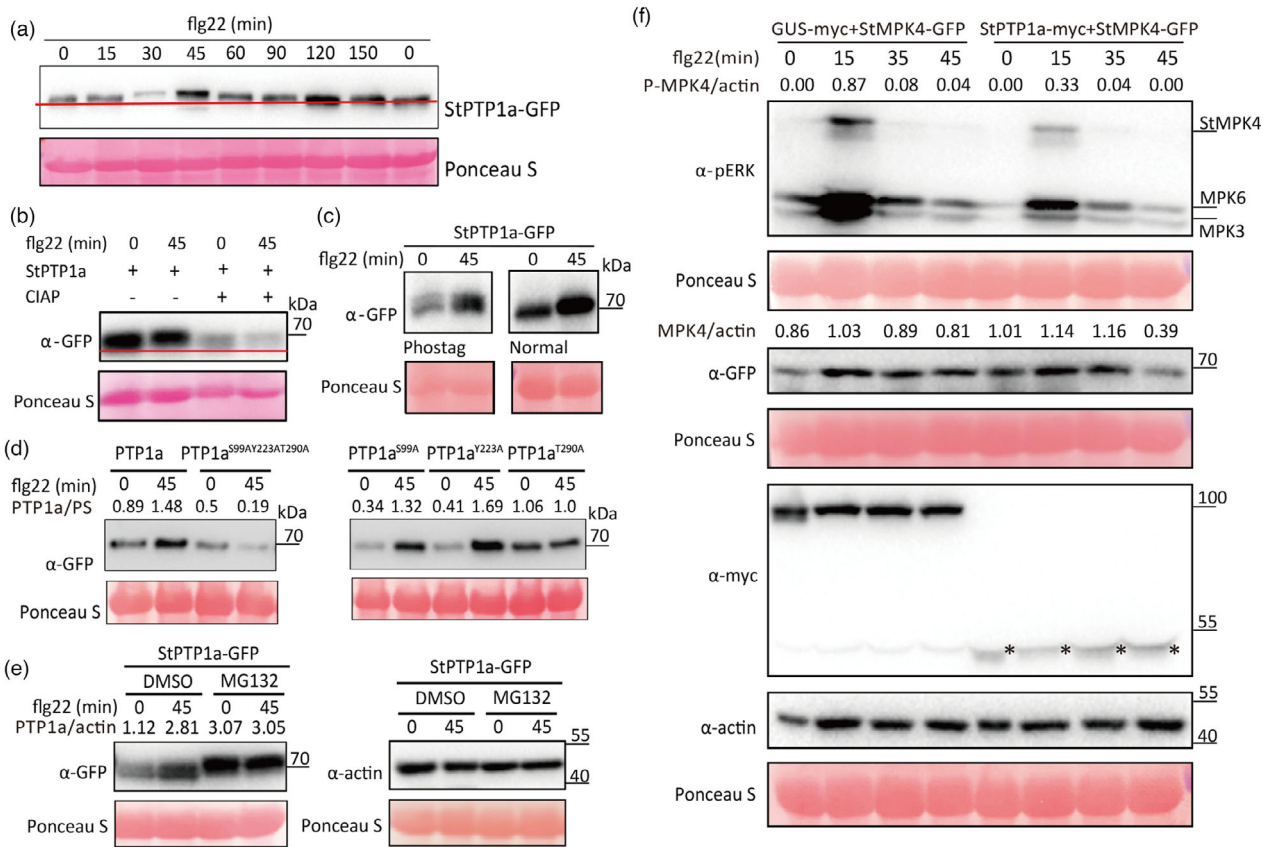

Figure 6 StPTP1a is phosphorylated and stabilized in response to flg22 treatment *in planta* and the timing of this phosphorylation corresponds with a decreased phosphorylation and activity of MPKs. (a) Four weeks old *N. benthamiana* leaves were agroinfiltrated with StPTP1a-GFP, and at 2 dpi the leaves were treated with flg22, after which total proteins were extracted at the indicated time points. Proteins were separated on SDS-PAGE gels and StPTP1a-GFP was detected using α-GFP antibody. (b, c) StPTP1a was agroinfiltrated into leaves of *N. benthamiana*, and at 2 dpi the leaves were treated with flg22, after which total proteins were extracted at 0 and 45 min after treatment. Protein extracts were treated either with (+) or without (−) the phosphatase CIAP (b). Phosphorylated StPTP1 is shown by a mobility shift of the bands on the Mn^{2+}-Phos-tag SDS-PAGE gel (c). Experiments were performed at least two times with similar results. (d) StPTP1a-GFP and StPTP1a^{S99AY223AT290A}-GFP (left panels) and StPTP1a^{S99A}-GFP, StPTP1a^{Y223A}-GFP and StPTP1a^{T290A}-GFP (right panels) were agroinfiltrated into leaves of *N. benthamiana*, and at 2 dpi the leaves were treated with flg22. Note that the StPTP1a-GFP, StPTP1a^{S99A}-GFP, StPTP1a^{Y223A}-GFP protein levels are stable, while the accumulation levels of StPTP1a^{S99AY223AT290A}-GFP and StPTP1a^{T290A} have decreased after flg22 treatment. (e) StPTP1a-GFP was agroinfiltrated into the leaves of *N. benthamiana*, and at 48 hpi the leaves were treated with 100 μM MG132 or its solvent 1% DMSO for 6 h before infiltrated with 10 μM flg22. The leaves were harvested at 0 or 45 min after flg22 treatments for protein isolation. Numbers above the blots indicate the relative intensity of StPTP1a bands to Rubisico (d) or plant actin (e). (f) StPTP1a suppresses MPK phosphorylation during PTI. GUS-myc or StPTP1a-myc was co-expressed with StMPK4-GFP into *N. benthamiana* leaves. At 2dpi the leaves were treated with flg22, and total proteins were extracted at the time points indicated. StMPK4 activation was detected using α-pERK antibody and the accumulation of GFP-tagged StMPK4 and myc-tagged StPTP1a is shown by using α-GFP and α-myc antibodies, plant actin detected by anti-actin antibody was shown as a loading control, respectively. Equal protein loading is indicated using Ponceau Staining. Numbers indicate the ratio of the intensity of phosphorylated StMPK4 or StMPK4-GFP proteins to the actin band signals. The recombinant fusion proteins of StPTP1a is marked with black asterisks. The experiments showed similar results in three biological replicates.

(Figure 6b). Interestingly, we also observed that StPTP1a was stabilized at 45 min after flg22 treatment (Figure 6c). To further confirm this, we transiently expressed StPTP1a-GFP or StPTP1a^{S99AY223AT290A}-GFP in *N. benthamiana* leaves and at 2 dpi the leaves were treated with flg22 and subsequently harvested after 0 and 45 min. Western blot analysis shows that the abundance of the StPTP1a protein is significantly increased at 45 min after flg22-treatment (Figure 6d), while the accumulation level of the mutant StPTP1a^{S99AY223AT290A}-GFP protein was lower at 45 min after flg22-treatment indicating that phosphorylation of StPTP1 is required for its stabilization. We did similar experiments using StPTP1a^{S99A}-GFP, StPTP1a^{Y223A}-GFP, and StPTP1a^{T290A}-GFP and observed that the protein levels of StPTP1a^{S99A}-GFP and StPTP1a^{Y223A}-GFP showed a significant increase at 45 min after flg22 treatment when compared to the 0 min control, while the accumulation of StPTP1a^{T290A}-GFP did not change significantly (Figure 6d). These results suggest that, in response to flg22, StPTP1a becomes phosphorylated at its S99, Y223 and T290 sites, which stabilizes the protein, resulting in a rapid increase in StPTP1a protein levels. To investigate whether the phosphorylation of StPTP1a repressed its degradation via the 26 S proteasome pathway, StPTP1a-GFP was expressed in *N. benthamiana* leaves for 48 h, before infiltration of the 26 S proteasome inhibitor MG132 or its solvent (1% DMSO). At 6 h after MG132 infiltration, the leaves were treated with 10 μM flg22. We observed that in the control DMSO-treated leaves

the abundance of the StPTP1a proteins is significantly increased at 45 min after flg22-treatment while in the MG132 treated leaves StPTP1a proteins are accumulated to the similar levels at 0 min and 45 min after flg22-treatment (Figure 6e). This result indicates that phosphorylation of StPTP1a stabilizes the protein through inhibition of 26 S proteasome-mediated degradation of StPTP1a. To determine whether dephosphorylation of StMPK7/4 by StPTP1a occurs during the onset of PTI, we co-expressed the control GFP/GUS-myc, or the StPTP1a-GFP/StPTP1a-myc protein, with myc-StMPK7/StMPK4-GFP and at 2 dpi the leaves were infiltrated with flg22. We observed that StMPK7/6/3 phosphorylation occurred over a period from 5 to 35 min after flg22 treatment, while the MPKs were gradually dephosphorylated within 60 min after flg22 treatment in the GFP co-expressing leaves. However, in StPTP1a-GFP co-expressing leaves, the maximum phosphorylation levels of the MPKs were lower and the turnover of the phosphorylated StMPK7 proteins occurred 15 min earlier than in the control. Phosphorylation of StMPK7 was still apparent at 35 min after flg22 treatment in the GFP co-expressing leaves, whereas this was hardly observed in the leaves in which StPTP1a was co-expressed (Figure S8a,c). Similarly, in StPTP1a-myc co-expressing leaves, the phosphorylation of StMPK4 was lower and their turnover was earlier than in the GUS-myc control (Figure 6f and Figure S8b,d). In addition, we also observed a significant accumulation of StMPK4 protein at PTI activation when compared to the 0 min control (Figure 6f). To examine whether the interaction of StPTP1a with StMKK1 or with StMPK7 is altered during the PTI response, we transiently co-expressed StPTP1a-nluc with cluc-StMKK1 or cluc-StMPK7 in *N. benthamiana* leaves, and at 2 dpi the leaves were infiltrated with flg22, infiltration of H_2O was used as the negative control. Leaves were harvested at 15 min after flg22 infiltration for LCI and we observed that the complemented luciferase fluorescence is similar for leaves infiltrated with flg22 or with H_2O (Figure S9), indicating that the mounting of PTI does not affect the interaction of StPTP1a with StMKK1 or StMPK7. Taken together, our results indicate that StPTP1a is phosphorylated upon the activation of PTI, which is correlated with an enhanced dephosphorylation of StMPK7 and StMPK4.

StMKK1 requires NbPTP1a to negatively regulate plant immunity

We further analysed whether StMKK1 depends on NbPTP1a for negative regulation of plant immunity by checking the infection levels by *P. infestans* and the suppression of *PR* gene expression in TRV-*NbPTP1a*- and TRV-*GUS*-inoculated plants upon transient expression of StMKK1. Agroinfiltration of GFP-StMKK1 in the TRV-*GUS*-inoculated plants significantly promotes *P. infestans* colonization and represses *PR1* and *PR2* gene expression, whereas in TRV-*NbPTP1a*-inoculated plants the expression of GFP-StMKK1 neither promotes pathogen colonization nor represses the expression of *PR* genes (Figure 7a–c). These results indicate that StPTP1a functions downstream of StMKK1, and is indeed required by StMKK1 to suppress plant defence responses.

Discussion

Uncontrolled MAPK signalling can result in severe defects in plant growth and development. Consequently, to avoid plant growth defects or spontaneous necrosis, the activation of MAPK cascades upon the onset of PTI is strictly regulated and again suppressed within a short time after its onset as a result of the activity of negative feedback loops. The suppression of MAPK cascade signalling largely depends on the activity of specific plant phosphatases. Our results show that the potato MAPKK StMKK1 interacts with, and phosphorylates, the potato tyrosine phosphatase StPTP1a at amino acid residues Ser-99, Tyr-223 and Thr-290, and that this phosphorylation increases the catalytic activity of StPTP1a. The potato MAPK StMPK7 and StMPK4 are downstream signalling targets of StMKK1, and StMPK7/4 activates plant SA-related immunity. StPTP1a in its turn dephosphorylates StMPK7/4 at Tyr-203, thereby suppressing StMPK signalling and compromising immunity to *Phytophthora* pathogens. Our results provide evidence that StPTP1a is directly activated by potato StMKK1 upon initiation of the PTI response and that activated StPTP1a dephosphorylates the StMKK1 downstream signalling components StMPK7 and StMPK4, thereby avoiding possible over-activation of the StMKK1-StMPK7/StMPK4 cascade. Our conclusions are supported by the fact that, although StMKK1 activates the positive immune regulators StMPK7 and StMPK4 (Zhang *et al.*, 2021), it still represses plant immunity, with SA-related immunity in particular (Chen *et al.*, 2021; Du *et al.*, 2021).

Plant tyrosine phosphatases participate in several multicellular signalling pathways, that is, salt stress, oxidative stress, wounding and challenge by pathogens. However, most studies concern DsPTPs, with only a few reports on tyrosine-specific PTPs (Shankar *et al.*, 2015). The catalytic activity of the Arabidopsis tyrosine-specific phosphatase AtPTP1 is inhibited by H_2O_2, similar to what has been reported for mammalian PTPs (Gupta and Luan, 2003; Lee and Esselman, 2002; Meng *et al.*, 2002). However, how phosphotyrosine-specific protein phosphatases are activated in plants remains unknown. Our results show that StMKK1 interacts with StPTP1a (Figure 1), and that this results in a direct phosphorylation of StPTP1a at Ser-99, Tyr-223 and Thr-290 by StMKK1 (Figure 3d). By introducing point mutations, we revealed that the phosphorylation of Ser-99, Tyr-223 and Thr-290 is essential for the activation of the phosphatase activity of StPTP1a (Figure 3). Our results, for the first time, reveal that plant phosphotyrosine-specific protein phosphatases are activated by phosphorylation. The Ser-99 is specifically present in PTPs from *Solanaceous* plants, while AtPTP1 contains a Glu residue at this position instead. This observation indicates that in Arabidopsis PTP1 may be activated through the phosphorylation of one or more amino acid residues different from those of potato StPTP1. Furthermore, whether there are additional protein kinases, next to MKK1, that are able to phosphorylate PTP1a *in planta* remains to be determined.

AtPTP1 was reported previously to dephosphorylate AtMPK6 and AtMPK4 (Huang *et al.*, 2000; Park *et al.*, 2011), and our study showed that StPTP1a dephosphorylates the orthologous proteins of AtMPK4 and AtMPK5 of potato, which is StMPK4 and StMPK7 (Figures 4 and 5), respectively. Whereas it does not dephosphorylate the orthologue of AtMPK6, StSIPK and the orthologue of AtMPK3, StWIPK (Figure 5b,c). This observation indicates that PTP1a may function differently in Arabidopsis and potato. Since the α-pERK antibody specifically detects the phosphorylation of Thr-202 and Tyr-204/203 of MPK proteins, StPTP1a likely dephosphorylates StMPK7/4 at Tyr203. The observation that StMPK7^{Y203A} and StMPK4^{Y203A} both no longer mediate immunity to *P. infestans* (Figure S7n,o and Figure 5j,k), that CA-StMPK7^{Y203A} and CA-StMPK4^{Y203A} have lost the ability to trigger cell death (Figure S7k–m and Figure 5i), and that StPTP1a inhibits

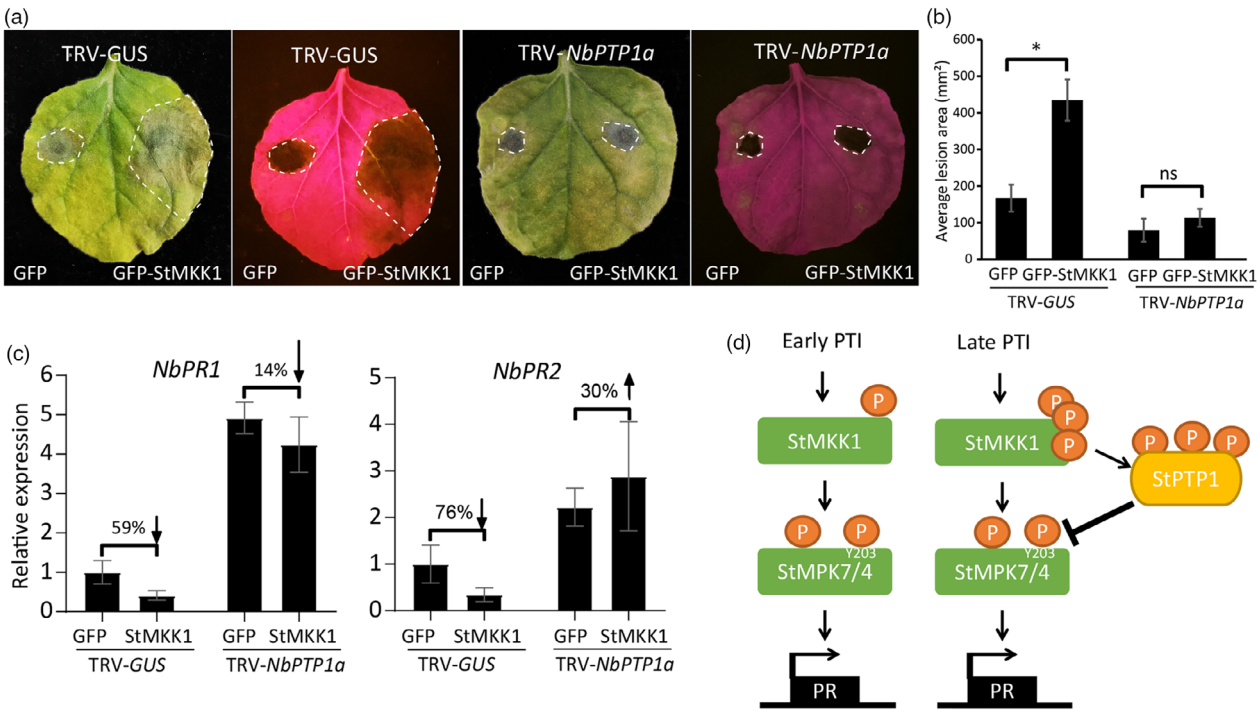

Figure 7 StMKK1 requires NbPTP1a for inhibiting plant immunity. (a, b) StMKK1 requires NbPTP1a for inhibiting resistance to *P. infestans*. *GFP* or *GFP-StMKK1* was agroinfiltrated into the left and right panels, respectively, of TRV-*GUS*- or TRV-*PTP1a*-inoculated leaves and after two days the infiltrated leaf areas were inoculated with *P. infestans*. The pictures showing lesion development were taken under normal light (left panels) or blue light (right panels) (a). Lesion diameters were determined at 6 dai, and the average lesion areas (mm^2) are shown in the graphs (b). Error bars indicate the standard error from at least 8 technical replicates. Significance is indicated with asterisks ($n \geq 8$; one-sided Student's *t*-test, one star indicates $P \leq 0.05$, ns indicates non-significant differences). (c) StMKK1 requires NbPTP1a for inhibiting *PR* gene expression. *GFP-StMKK1* or *GFP* was transiently expressed in leaves of TRV-*GUS*- or TRV-*PTP1a*-inoculated *N. benthamiana* plants, and the leaves were harvested at 2 dpi for RNA isolation. The qRT-PCR results show the expression of *NbPR1* and *NbPR2* in both TRV-*GUS*- and TRV-*PTP1a*-inoculated plants. Note that VIGS of *NPTP1a* hampers the capacity of StMKK1 to suppress *PR* gene expression. The experiments were repeated at least three times with similar results. (d) The dual functions of StMKK1. Upon early PTI activation, activated StMKK1 phosphorylates and activates its downstream targets, StMPK7/4, which in their turn activate downstream *PR* gene expression. However, after PTI initiation, activated StMKK1 also interacts with, and phosphorylates, the phosphatase StPTP1a, which activates the phosphatase and, in its turn, mediates the dephosphorylation of StMPK7/4 at Tyr-203, thereby repressing *PR* gene expression.

constitutively activated CA-StMPK7/4-triggered cell death and immunity (Figure S7a–c and Figure 5h), confirmed this hypothesis. Different from the Arabidopsis DsPTPase AtMKP1, which was found to be phosphorylated and activated by its substrate, AtMPK6 (Jiang *et al.*, 2017; Park *et al.*, 2011), StPTP1a is not phosphorylated and activated by its substrate, StMPK7 (Figure 4e).

We found that the transgenic potato lines constitutively silenced for *StPTP1a/b* show an enhanced MPK activation (Figure 2k), activated SA-related signalling (Figure 2l) and severe dwarfism (Figure 2i), which is similar to the findings in Arabidopsis that the *mkp1ptp1* double mutant showed enhanced SA-related gene expression and dwarfism when compared to *mkp1* knockout plants (Bartels *et al.*, 2009). StMPK7 positively regulates plant immunity to *P. infestans* by activating SA-related gene expression (Zhang *et al.*, 2021), and AtMPK4, AtMPK6 and SlMKK4 were also found to activate plant SA-related immunity (Chai *et al.*, 2014; Li *et al.*, 2014b; Pitzschke *et al.*, 2009). Probably, due to the silencing of *PTP1*, the phosphorylation status of the MPK7/4 proteins remains at elevated levels, resulting in overactivation of the immune response, which in its turn causes developmental aberrations. Another possibility is that StPTP1 may have additional substrates that play a role in plant development and are overactivated when *PTP1* is silenced. The role of tyrosine-specific phosphatases in plants is largely underestimated, and whether StPTP1 regulates other cellular processes next to the immune response, remains to be elucidated.

Phosphorylation of StPTP1a is required for its catalytic activity, and the suppression of both PTI activation and SA-related gene expression (Figure 2). Similar to AtMKP1, for which it has been shown that its phosphorylation significantly enhances its stability (Jiang *et al.*, 2017), our results show that phosphorylation of StPTP1a significantly enhances its catalytic activity (Figure 3) and stability (Figure 6c,d). StPTP1a^{S99A}, StPTP1a^{T290A} and StPTP1a^{Y223A} showed different levels of stabilization upon their phosphorylation, whereas StPTP1a^{S99AY223AT290A} does not (Figure 6d). Our results show that StPTP1a is phosphorylated, and thereby activated during PTI (Figure 6a). StPTP1a activation occurred within 10–15 min after MPK activation (Figure 6f and Figure S8), suggesting that StPTP1a is activated during PTI to suppress MPK phosphorylation, thereby avoiding MPK overactivation. Taken together, our research revealed that StPTP1a is activated by StMKK1 during the onset of PTI and that thereby StMKK1 plays a dual role in plant immunity. In response to triggering PTI, StMKK1 phosphorylates and thereby activates StMPK7/4, however after PTI initiation StMKK1 also

phosphorylates and activates StPTP1a, which leads to the suppression of MPK7/4 activation by StPTP1a as a result of their dephosphorylation (Figure 7d). This tight regulation of StMPK7/4 activation by the negative feed-back loop facilitated by StMKK1-mediated activation of the negative regulator StPTP1a might enable the plant to avoid overactivation of the immune response and balances plant growth and defence trade-offs. Our findings also explain the conflicting observations concerning the role of StMKK1 in plant immunity; this MAPKK indeed participates in PTI signalling and activates StMPK7/4, thereby acting as a positive regulator. However, its overexpression does not promote plant immunity but rather suppresses it, since StMKK1 also activates the protein tyrosine phosphatase StPTP1a, which inactivates StMPK7/4 by their dephosphorylation.

Experimental procedures

Plasmid construction

StPTP1a (PGSC0003DMC400045325) was PCR-amplified using a cDNA library of potato cultivar Desiree as a template. For protein–protein interaction assays, the *StPTP1a-GFP* and *StPTP1a-myc* plasmids were generated by inserting the *StPTP1a* gene in the vector pART27-GFP or pART27-myc, respectively, using *Xho*I/*Hin*dIII sites. The *StPTP1a-nluc* plasmid was generated by inserting *StPTP1a* gene in the vector pCAMBIA-nluc using the *Kpn*I and *Sal*I restriction sites. For phosphatase activity assays, the mutant *StPTP1aAS* (*StPTP1a*$^{D243A,\ C274S}$) was generated, with a mutation of two catalytically essential amino acids, by overlap PCR using *StPTP1a-myc* as a template. *GFP*, *StPTP1a*, *StPTP1aAS* and *StMKK1* were inserted into the pET21a-His-MBP or pET32a-His vector with, respectively, the *Eco*RI/*Xho*I or *Nco*I/*Xho*I restriction sites, to generate the *His-MBP-StPTP1a*, *His-MBP-GFP* and *His-MBP-StPTP1aAS*. The *GST-StMPK7* plasmid was generated by inserting *StMPK7* into the vector pGEX-6P-1, using the *Bam*HI/*Sal*I sites. A 289 bp DNA fragment of *StPTP1* was PCR-amplified and the sense fragment was ligated into the 35 s-pART27 vector with restriction enzymes *Xho*I and *Kpn*I, and subsequently the antisense *StPTP1* DNA fragment was cloned into the same vector, using *Xba*I and *Hin*dIII sites to generate the RNA interference (RNAi) vector named StPTP1-RNAi. All the used primers were shown in Table S1.

Virus-Induced gene silencing (VIGS)

The *NbPTP1a/b* orthologous genes were selected by a BLAST search using the *StPTP1a* gene sequence in the Sol genomics network database (https://solgenomics.net/). The *NbPTP1a* gene fragment targeting *Niben101Scf03425g03015* and *Niben101Scf01365g00010*, and the *NbPTP1b* gene fragment targeting *Niben101Scf04216g01006* were obtained by PCR using a *N. benthamiana* cDNA library as a template, with the primers shown in Table S1, and the PCR fragment was inserted into the TRV2 vector using *Eco*RI/*Bam*HI, to generate the TRV-*NbPTP1a* and TRV-*NbPTP1b* plasmids. The TRV1 (TRV-*RNA1*) or TRV2 (TRV-*RNA2*) plasmids were transformed into Agrobacterium strain C58C1 and mixed in a 1:1 ratio to a final OD600 of 0.6 for agroinfiltration. Two weeks old *N. benthamiana* seedlings were agroinfiltrated with TRV-*NbPTP1a* or TRV-*GUS*, and 3 weeks after agroinfiltration the silencing efficiency was determined.

Potato transformation and plant growth conditions

The potato cultivar Desiree was used for transformation as described by Sun *et al*. (2016). Independent transgenic potato lines, and *N. benthamiana* plants were grown at 25°C, under a 16/8 h day/night cycle with 45% relative humidity (RH) in a climate chamber.

Agroinfiltration

The agrobacterium strain C58C1 was cultured at 28°C in LB medium with the appropriate antibiotics for 2 days. The bacteria were collected by centrifugation at 1000 g for 10 min, after which they were re-suspended in infiltration medium as described by Van der Hoorn *et al*. (2000). The density of the bacterial suspension was adjusted to an OD600 of 0.3 for most of the agroinfiltration assays, whereas an OD600 of 0.6 was used for cell death suppression assays.

Detached leaf assays

The fully expanded middle two or three leaves of four-week-old *N. benthamiana* plants and the fifth to seventh leaf counted from the bottom of VIGSed plants were selected for detached leaf assays. *P. infestans* isolate 14-3-GFP was grown on rye sucrose agar medium for about 10 days and zoospores were harvested for inoculation assays. For each inoculation, about 1000 zoospores were applied onto the leaves, and the leaves were kept at 100% RH at 18°C, for a few days before lesion diameters were measured.

Yeast Two-Hybrid assays

The BD plasmid pGBKT7:StMKK1 was transformed into *Saccharomyces cerevisiae* strain Y187, and yeast two-hybrid (Y2H) screenings were performed according to the protocol described in the Matchmaker™ GAL4 Two-Hybrid System 3 & Libraries User Manual (Clontech). For one-to-one Y2H assays, the BD vector pGBKT7 was co-transformed with the AD vector pGADT7 into the yeast strain AH109. Interaction was confirmed by growing the yeast transformants on QDO (selective drop-out/−Trp-Leu-His-Ade) medium. Positive and negative interaction controls were provided by the Matchmaker™ GAL4 Two-Hybrid System 3 (Clontech).

Protein–Protein interaction assays

For co-immunoprecipitation assays, leaves were harvested at 2 days post agroinfiltration and total proteins were extracted with GTEN buffer as described by Tameling and Baulcombe (2007). About 1.8 mL of total protein extract was incubated with 12 μL GFP-trap_A beads (Chromotek) at 4°C for 1.5 h. For firefly luciferase complementation imaging (LCI) assays, StPTP1a-nluc was co-agroinfiltrated with cluc-StMKK1 into *N. benthamiana* leaves, and co-expression of StMKK1-nluc with cluc-PITG20303 was used as a positive control (Du *et al*., 2021). At 2 dpi, leaves were harvested and the LCI experiment was performed according to the protocol described by Chen *et al*. (2008).

Recombinant protein purification and *in vivo* and *in vitro* phosphorylation assays

His-MBP-GFP-, His-MBP-StPTP1a-, His-MBP-StPTP1aAS-, GST-StMPK7- and His-StMKK1 constructs were transformed to *Escherichia coli* strain BL21-CodonPlus (DE3) and proteins were purified as described by Fan *et al*. (2018). The *in vitro*

phosphorylation assay was performed according to the protocol as described by Li *et al*. (2014a) with minor modifications. About 2 μg of His-StMKK1 and GST-StMPK7 were incubated with 2 μg of His-MBP-GFP, His-MBP-StPTP1a or His-MBP-StPTP1aAS, in 20 μL reaction buffer (25 mM Tris–HCl (pH 7.5), 10 mM $MgCl_2$, 1 mM DTT and 100 μM dATP), for 30 min at 30°C. For phos-tag assays the samples were separated on SDS-PAGE gels (8%) containing 100 μM $MnCl_2$ and 100 μM phos-tag (FUJIFILM Wako, AAL-107). The His-MBP-StPTP1a phosphorylation was visualized with anti-MBP antibodies. For the *in vivo* phosphorylation assay, 4 weeks old *N. benthamiana* leaves were infiltrated with 10 μM flg22 solution to induce MPK protein activation. Total proteins were extracted in GTEN buffer containing phosphatase inhibitor cocktails 2 & 3 (1:100 dilution, P5726 & P0044, Sigma) and protease inhibitor cocktail (1 tablet for 50 mL GTEN), and MPK protein activation was detected with anti-pERK (#4370, Cell Signaling) antibodies.

Identification of protein phosphorylation sites

To identify the phospho-sites of StPTP1a *in vitro*, 20 μg of the purified MBP-StPTP1a protein was first treated with 1 μg CIAP (calf intestine alkaline phosphatase) in 200 μL phosphatase buffer, for 10 min at 37°C. The CIAP was inactivated at 80°C for 2 min, and subsequently the dephosphorylated MBP-StPTP1a protein was incubated with 5 μg of His-StMKK1 and the *in vitro* kinase assay was performed at 37°C, overnight. Phosphorylated MBP-StPTP1a was then precipitated with acetone, and digested by trypsin and subjected to mass spectrometry to identify the phosphorylation sites that are directly phosphorylated by StMKK1.

Western blot analyses

Proteins were separated on SDS-PAGE gels (10%), before being transferred to Immune-Blot PVDF membranes (Roche). Subsequently, the membranes were incubated in blocking buffer for 2 h at 4°C. After blocking, the membranes were incubated with anti-His (#AE003, ABclonal), anti-GFP (#AE011, ABclonal), anti-GST (#AE006, ABclonal), anti-MBP (#AE016, ABclonal), anti-myc (#AE009, ABclonal), anti-actin (#AC009, ABclonal) antibodies for 2 h at 4°C. The membranes were subsequently washed with blocking buffer for three times, before being incubated with the secondary antibody HRP goat anti-rabbit IgG (H + L) antibody (#AS014, ABclonal), or HRP goat anti-mouse IgG (H + L) antibody (#AS003, ABclonal). Finally, the membranes were washed with TBST and they were developed using the eECL western blot kit (CWBIO, Beijing, China).

PTP activity assay

The phosphatase activity of StPTP1a and StPTP1aAS was detected according to the protocol described by Chen *et al*. (2017), with minor modifications. Phosphatase activity was determined by adding 2 μg of MBP-GFP, MBP-StPTP1a or MBP-StPTP1aAS protein to 100 μL of reaction buffer (2 mM pNPP, 2.5 mM EDTA and 2.5 mM sodium acetate, pH 5.2), followed by incubation at 37°C for 5 min.

DAB staining and ion leakage assays

N. benthamiana leaves were harvested and incubated in diaminobenzidine (DAB) staining solution (1 mg/mL DAB dissolved in MQ, pH3.7) for about 12 h. Then the leaves were incubated in 70% ethanol to remove the chlorophyll, after which pictures were taken. The relative ion leakage was measured according to the protocol described by Bouwmeester *et al*. (2014).

Gene expression assays

Total RNA was extracted (E.Z.N.A.) Plant RNA Kit (#R6827-01, OMEGA), and the first strand cDNA was synthesized using 1 μg of total RNA according to the instructions from PrimeScript RT reagent Kit (TaKaRa). The qRT-PCRs were performed, and gene expression levels were quantified, according to the method described by Li *et al*. (2019). The primer pairs that were used are shown in Table S1.

Accession numbers

Accession numbers are as follows: StPTP1a, PGSC0003 DMC400045325; StPTP1b, Sotub06g024510; StMPK7, PGSC000 3DMP400021542; StMKK1, Sotub12g010200; NbPTP1a, Niben101Scf03425g03015 and Niben101Scf01365g00010; NbP TP1b, Niben101Scf04216g01006.

Funding

This work was supported by the National Science Foundation of China (32072401), the Chinese Universities Scientific Fund (2452018028 and 2452017069) and the Program of Introducing Talents of Innovative Discipline to Universities (Project 111), from the State Administration of Foreign Experts Affairs (#B18042).

Acknowledgements

We would like to thank the Horticulture Science Research Center of Northwest A&F University for providing their advanced facilities; Dr. Qiong Zhang and Technician Xiaona Zhou of CSBAA for assistance with high-sensitivity LC–MS/MS (QExactive HF-X, Thermo Fisher, Waltham, MA).

Author contributions

Y.D. designed the research. F.L., X.C., R.Y. and K.Z. performed the experiments. F.L. and X.C. analysed the data. Y.D., M.H.A.J.J. and W.S. wrote the manuscript. All authors reviewed the manuscript.

Conflict of interest

The authors declare no conflict of interest.

Data availability statement

Data sharing is not applicable as no new data were created or analysed in this study.

References

Ahsan, N., Wilson, R.S., Rao, R.S.P., Salvato, F., Sabila, M., Ullah, H. and Miernyk, J.A. (2020) Mass spectrometry-based identification of phospho-tyr in plant proteomics. *J. Proteome Res.* **19**, 561–571.

Bartels, S., Anderson, J.C., Besteiro, M.A.G., Carreri, A., Hirt, H., Buchala, A., Metraux, J.P. *et al*. (2009) MAP kinase phosphatase1 and protein tyrosine phosphatase1 are repressors of salicylic acid synthesis and SNC1-mediated responses in *Arabidopsis*. *Plant Cell* **21**, 2884–2897.

Bi, G.Z., Zhou, Z.Z., Wang, W.B., Li, L., Rao, S.F., Wu, Y. *et al*. (2018) Receptor-like cytoplasmic kinases directly link diverse pattern recognition receptors to

the activation of mitogen-activated protein kinase cascades in *Arabidopsis*. *Plant Cell* **30**, 1543–1561.
Bojar, D., Martinez, J., Santiago, J., Rybin, V., Bayliss, R. and Hothorn, M. (2014) Crystal structures of the phosphorylated BRI1 kinase domain and implications for brassinosteroid signal initiation. *Plant J.* **78**, 31–43.
Bouwmeester, K., Han, M., Blanco-Portales, R., Song, W., Weide, R., Guo, L.Y., van der Vossen, E.A.G. *et al*. (2014) The Arabidopsis lectin receptor kinase LecRK-I.9 enhances resistance to *Phytophthora infestans* in Solanaceous plants. *Plant Biotechnol. J.* **12**, 10–16.
Bukczynska, P., Klingler-Hoffmann, M., Mitchelhill, K.I., Lam, M.H.C., Ciccomancini, M., Tonks, N.K., Sarcevic, B. *et al*. (2004) The T-cell protein tyrosine phosphatase is phosphorylated on Ser-304 by cyclin-dependent protein kinases in mitosis. *Biochem. J.* **380**, 939–949.
Chai, J.Y., Liu, J., Zhou, J. and Xing, D. (2014) Mitogen-activated protein kinase 6 regulates NPR1 gene expression and activation during leaf senescence induced by salicylic acid. *J. Exp. Bot.* **65**, 6513–6528.
Chen, C., Liang, F., Chen, B., Sun, Z.Y., Xue, T.D., Yang, R.L. and Luo, D.Q. (2017) Identification of demethylincisterol A(3) as a selective inhibitor of protein tyrosine phosphatase Shp2. *Eur. J. Pharmacol.* **795**, 124–133.
Chen, H.M., Zou, Y., Shang, Y.L., Lin, H.Q., Wang, Y.J., Cai, R., Tang, X.Y. *et al*. (2008) Firefly luciferase complementation imaging assay for protein-protein interactions in plants. *Plant Physiol.* **146**, 368–376.
Chen, X., Wang, W., Cai, P., Wang, Z., Li, T. and Du, Y. (2021) The role of the MAP kinase-kinase protein StMKK1 in potato immunity to different pathogens. *Hortic Res.* **8**, 117.
Dadke, S., Kusari, A. and Kusari, J. (2001) Phosphorylation and activation of protein tyrosine phosphatase (PTP) 1B by insulin receptor. *Mol. Cell. Biochem.* **221**, 147–154.
Du, Y., Chen, X.K., Guo, Y.L., Zhang, X.J., Zhang, H.X., Li, F.F., Huang, G.Y. *et al*. (2021) *Phytophthora infestans* RXLR effector PITG20303 targets a potato MKK1 protein to suppress plant immunity. *New Phytol.* **230**, 878–515.
Fan, G., Yang, Y., Li, T., Lu, W., Du, Y., Qiang, X., Wen, Q. *et al*. (2018) A *Phytophthora capsici* RXLR effector targets and inhibits a plant PPIase to suppress endoplasmic reticulum-mediated immunity. *Mol. Plant* **11**, 1067–1083.
Flint, A.J., Gebbink, M.F., Franza, B.R., Jr., Hill, D.E. and Tonks, N.K. (1993) Multi-site phosphorylation of the protein tyrosine phosphatase, PTP1B: identification of cell cycle regulated and phorbol ester stimulated sites of phosphorylation. *EMBO J.* **12**, 1937–1946.
Fu, S.F., Lin, C.W., Kao, T.W., Huang, D.D. and Huang, H.J. (2011) *PaPTP1*, a gene encoding protein tyrosine phosphatase from orchid, phalaenopsis amabilis, is regulated during floral development and induced by wounding. *Plant Mol Biol Rep.* **29**, 106–116.
Gao, M., Liu, J., Bi, D., Zhang, Z., Cheng, F., Chen, S. and Zhang, Y. (2008) MEKK1, MKK1/MKK2 and MPK4 function together in a mitogen-activated protein kinase cascade to regulate innate immunity in plants. *Cell Res.* **18**, 1190–1198.
Gupta, R. and Luan, S. (2003) Redox control of protein tyrosine phosphatases and mitogen-activated protein kinases in plants. *Plant Physiol.* **132**, 1149–1152.
Huang, Y.F., Li, H., Gupta, R., Morris, P.C., Luan, S. and Kieber, J.J. (2000) ATMPK4, an Arabidopsis homolog of mitogen-activated protein kinase, is activated in vitro by AtMEK1 through threonine phosphorylation. *Plant Physiol.* **122**, 1301–1310.
Jiang, L.Y., Anderson, J.C., Besteiro, M.A.G. and Peck, S.C. (2017) Phosphorylation of Arabidopsis MAP kinase phosphatase 1 (MKP1) is required for PAMP responses and resistance against Bacteria. *Plant Physiol.* **175**, 1839–1852.
Lee, K. and Esselman, W.J. (2002) Inhibition of PTPs by H_2O_2 regulates the activation of distinct MAPK pathways. *Free Radic Biol.* **33**, 1121–1132.
Li, L., Li, M., Yu, L.P., Zhou, Z.Y., Liang, X.X., Liu, Z.X., Cai, G.H. *et al*. (2014a) The FLS2-associated kinase BIK1 directly phosphorylates the NADPH oxidase RbohD to control plant immunity. *Cell Host Microbe* **15**, 329–338.
Li, T.T., Wang, Q.H., Feng, R.R., Li, L.C., Ding, L.W., Fan, G.J., Li, W.W. *et al*. (2019) Negative regulators of plant immunity derived from cinnamyl alcohol dehydrogenases are targeted by multiple *Phytophthora* Avr3a-like effectors. *New Phytol.* **20**, 2231–2429. https://doi.org/10.1111/nph.16139
Li, X.H., Zhang, Y.F., Huang, L., Ouyang, Z.G., Hong, Y.B., Zhang, H.J., Li, D.Y. *et al*. (2014b) Tomato SlMKK2 and SlMKK4 contribute to disease resistance against *Botrytis cinerea*. *BMC Plant Biol.* **14**, 166.
Lin, H., Wang, M., Chen, Y., Nomura, K., Hui, S., Gui, J., Zhang, X. *et al*. (2022) An MKP-MAPK protein phosphorylation cascade controls vascular immunity in plants. *Sci. Adv.* **8**, eabg8723.
Liu, Z., Mei, E., Tian, X., He, M., Tang, J., Xu, M., Liu, J. *et al*. (2021) OsMKKK70 regulates grain size and leaf angle in rice through the OsMKK4-OsMAPK6-OsWRKY53 signaling pathway. *J. Integr. Plant Biol.* **63**, 2043–2057.
Lu, Y.Y., Su, W.L., Bao, Y., Wang, S., He, F., Wang, D.L., Yu, X.Q. *et al*. (2020) Poplar *PdPTP1* gene negatively regulates salt tolerance by affecting ion and ROS homeostasis in *Populus*. *Int. J. Mol. Sci.* **21**, 1065.
Luan, S. (2003) Protein phosphatases in plants. *Annu. Rev. Plant Biol.* **54**, 63–92.
Maehama, T., Taylor, G.S. and Dixon, J.E. (2001) PTEN and myotubularin: novel phosphoinositide phosphatases. *Annu. Rev. Biochem.* **70**, 247–279.
Meng, T.C., Fukada, T. and Tonks, N.K. (2002) Reversible oxidation and inactivation of protein tyrosine phosphatases in vivo. *Mol. Cell* **9**, 387–399.
Moorhead, G.B.G., De Wever, V., Templeton, G. and Kerk, D. (2009) Evolution of protein phosphatases in plants and animals. *Biochem. J.* **417**, 401–409.
Mühlenbeck, H., Bender, K.W. and Zipfel, C. (2021) Importance of tyrosine phosphorylation for transmembrane signaling in plants. *Biochem. J.* **478**, 2759–2774.
Park, H.C., Song, E.H., Nguyen, X.C., Lee, K., Kim, K.E., Kim, H.S., Lee, S.M. *et al*. (2011) Arabidopsis MAP kinase phosphatase 1 is phosphorylated and activated by its substrate AtMPK6. *Plant Cell Rep.* **30**, 1523–1531.
Pitzschke, A., Djamei, A., Bitton, F. and Hirt, H. (2009) A major role of the MEKK1-MKK1/2-MPK4 pathway in ROS signalling. *Mol. Plant* **2**, 120–137.
Popescu, S.C., Popescu, G.V., Bachan, S., Zhang, Z.M., Gerstein, M., Snyder, M. and Dinesh-Kumar, S.P. (2009) MAPK target networks in *Arabidopsis thaliana* revealed using functional protein microarrays. *Gene Dev.* **23**, 80–92.
Shankar, A., Agrawal, N., Sharma, M., Pandey, A. and Pandey, G.K. (2015) Role of protein tyrosine phosphatases in plants. *Curr. Genomics* **16**, 224–236.
Sun, K., Wolters, A.M.A., Vossen, J.H., Rouwet, M.E., Loonen, A.E.H.M., Jacobsen, E., Visser, R.G.F. *et al*. (2016) Silencing of six susceptibility genes results in potato late blight resistance. *Transgenic Res.* **25**, 731–742.
Tameling, W.I.L. and Baulcombe, D.C. (2007) Physical association of the NB-LRR resistance protein Rx with a ran GTPase-activating protein is required for extreme resistance to *Potato virus X*. *Plant Cell* **19**, 1682–1694.
Ueno, Y., Yoshida, R., Kishi-Kaboshi, M., Matsushita, A., Jiang, C.J., Goto, S., Takahashi, A. *et al*. (2015) Abiotic stresses antagonize the rice defence pathway through the tyrosine-dephosphorylation of OsMPK6. *PLoS Pathog.* **11**, e1005231.
Van der Burgh, A.M. and Joosten, M. (2019) Plant immunity: thinking outside and inside the box. *Trends Plant Sci.* **24**, 587–601.
Van der Hoorn, R.A.L., Laurent, F., Roth, R. and De Wit, P.J.G.M. (2000) Agroinfiltration is a versatile tool that facilitates comparative analyses of Avr9/Cf-9-induced and Avr4/Cf-4-induced necrosis. *Mol. Plant Microbe Interact.* **13**, 439–446.
Xu, Q., Fu, H.F., Gupta, R. and Luan, S. (1998) Molecular characterization of a tyrosine-specific protein phosphatase encoded by a stress-responsive gene in *Arabidopsis*. *Plant Cell* **10**, 1769–1857.
Zhang, H.X., Li, F.F., Li, Z.Z., Cheng, J., Chen, X.K., Wang, Q.H., Joosten, M.H.A.J. *et al*. (2021) Potato StMPK7 is a downstream component of StMKK1 and promotes resistance to the oomycete pathogen *Phytophthora infestans*. *Mol. Plant Pathol.* **22**, 644–657.
Zhang, M. and Zhang, S. (2022) Mitogen-activated protein kinase cascades in plant signaling. *J. Integr. Plant Biol.* **64**, 301–341.
Zhang, Z., Wu, Y., Gao, M., Zhang, J., Kong, Q., Liu, Y., Ba, H. *et al*. (2012) Disruption of PAMP-induced MAP kinase cascade by a *Pseudomonas syringae* effector activates plant immunity mediated by the NB-LRR protein SUMM2. *Cell Host Microbe* **11**, 253–263.
Zhang, Z.B., Liu, Y.N., Huang, H., Gao, M.H., Wu, D., Kong, Q. and Zhang, Y.L. (2017) The NLR protein SUMM2 senses the disruption of an immune signaling MAP kinase cascade via CRCK3. *EMBO Rep.* **18**, 292–302.

Supporting information

Additional supporting information may be found online in the Supporting Information section at the end of the article.

Figure S1 Phylogenetic analysis of PTP1a proteins.
Figure S2 StPTP1a negatively regulates immunity to Phytophthora pathogens.
Figure S3 Morphology of *N. benthamiana* plants inoculated with TRV-*NbPTP1*, and silencing efficiency of the endogenous *PTP1* genes.
Figure S4 Amino acid sequence alignment of PTP1 proteins.
Figure S5 Purification of recombinant PTP1a proteins from *E. coli* and determination of their phosphatase activity.
Figure S6 StPTP1aAS, StPTP1a^{S99A}, StPTP1a^{Y223A}, StPTP1a^{T290A} and StPTP1a^{S99AY223AT290A} have lost their ability to suppress plant immunity to *P. infestans*.
Figure S7 StPTP1a represses CA-StMPK7-induced cell death and StMPK7-mediated SA-related immunity.
Figure S8 StPTP1a is activated during PTI to turn over the MPK activation.
Figure S9 Treatment with flg22 does not affect the interaction between StPTP1a and StMKK1, or StMPK7.
Figure S10 Silencing of *NbPTP1a* increased the phosphorylation of StMPK7 and StMPK4.
Table S1 Sequences of the primers used in this study.